# Optogenetic control of PRC1 reveals its role in chromosome alignment at the metaphase plate

Mihaela Jagrić[1#], Patrik Risteski[1#], Jelena Martinčić[1#], Ana Milas[1], Iva M. Tolić[1*]

[1]Division of Molecular Biology, Ruđer Bošković Institute, Bijenička cesta 54, 10000 Zagreb, Croatia

[#]These authors contributed equally to this work.

[*]Corresponding author: I.M.T. (tolic@irb.hr)

## Abstract

During metaphase, chromosome position at the spindle equator is mainly regulated by the forces exerted by kinetochore microtubules. However, the role of forces arising from mechanical coupling between sister kinetochore fibers and bridging fibers, whose antiparallel microtubules are crosslinked by protein regulator of cytokinesis 1 (PRC1), in chromosome alignment is unknown. Here we develop an optogenetic approach for acute removal of PRC1 and show that PRC1 promotes kinetochore alignment. PRC1 removal resulted in reduction of bridging fibers and straightening of outermost kinetochore fibers. The inter-kinetochore distance decreased, the metaphase plate widened, and lagging kinetochores appeared, suggesting a role of PRC1 in regulating forces on kinetochores. MKLP1/kinesin-6 was lost from the spindle together with PRC1, whereas Kif4A/kinesin-4 remained on chromosomes and CLASP1, Kif18A/kinesin-8, and CENP-E/kinesin-7 on kinetochore fiber tips. We conclude that in metaphase PRC1, by mechanically coupling bridging and kinetochore fibers, regulates spindle mechanics and buffers kinetochore movements, promoting chromosome alignment.

Chromosome alignment at the spindle equator in metaphase is a distinctive feature of mitosis. Chromosome congression to the metaphase plate has been explored extensively (Barisic et al., 2014; Cai et al., 2009; Kapoor et al., 2006; Maiato et al., 2017), but less understood is the maintenance of chromosome alignment, which depends on forces exerted by kinetochore fibers (k-fibers) and polar ejection forces (Armond et al., 2015; Stumpff et al., 2008; Stumpff et al., 2012; Wandke et al., 2012). However, sister k-fibers are connected by a bridging fiber, which consists of antiparallel microtubules crosslinked by protein regulator of cytokinesis 1 (PRC1) (Kajtez et al., 2016; Polak et al., 2017; Vukusic et al., 2017), and the role of forces arising from mechanical coupling between k-fibers and bridging fibers in chromosome alignment at the metaphase plate is unknown.

PRC1, like other non-motor microtubule-associated proteins from Ase1/PRC1/MAP65 family, selectively bundles antiparallel microtubules and provides stable overlaps *in vitro* (Bieling et al., 2010; Janson et al., 2007; Mollinari et al., 2002; Subramanian et al., 2010). Cellular studies of its function show that PRC1 is associated with the spindle midzone in anaphase, where its activity is essential for stable microtubule organization, localization of numerous microtubule-associated proteins within this structure, and successful completion of cytokinesis, while its microtubule-binding and -bundling affinities are regulated by phosphorylation and dephosphorylation events (Gruneberg et al., 2006; Jiang et al., 1998; Kurasawa et al., 2004; Liu et al., 2009; Mollinari et al., 2002; Mollinari et al., 2005; Neef et al., 2007; Subramanian et al., 2013; Subramanian et al., 2010; Zhu and Jiang, 2005; Zhu et al., 2006). In metaphase PRC1 crosslinks microtubules within bridging fibers, which laterally link sister k-fibers (Kajtez et al., 2016; Polak et al., 2017; Tolic, 2018).

In this work, we developed an optogenetic approach for acute and reversible removal of PRC1 from the spindle to the cell membrane, building upon ideas of dimerization or dissociation induced chemically (Cheeseman et al., 2013; Haruki et al., 2008; Robinson et al., 2010; Wordeman et al., 2016) or by light (Fielmich et al., 2018; Guntas et al., 2015; Okumura et al., 2018; van Haren et al., 2018; Yang et al., 2013; Zhang et al., 2017) to rapidly redistribute proteins. By using our assay on metaphase spindles, we found that PRC1 promotes kinetochore alignment. PRC1 removal resulted in partial disassembly of bridging fibers and change of spindle shape, demonstrating a role of bridging fibers in the spindle force balance. Moreover, the metaphase plate widened, inter-kinetochore distance decreased, and lagging chromosomes appeared more frequently, showing that PRC1 regulates forces acting on kinetochores. PRC1 removal during metaphase resulted in loss of MKLP1/kinesin-6 from

the spindle, but it did not affect the localization of Kif4A/kinesin-4 on the chromosomes and CLASP1, Kif18A/kinesin-8, and CENP-E/kinesin-7 on the plus ends of k-fibers. In conclusion, our optogenetic experiments show that in metaphase PRC1 crosslinks k-fibers with bridging microtubules, thereby regulating spindle mechanics and limiting the extent of kinetochore movements, which promotes chromosome alignment.

## RESULTS

### Optogenetic system for fast and reversible removal of PRC1 from the metaphase spindle

To study the role of PRC1 and the forces arising from coupling of bridging and k-fibers in chromosome alignment, we developed an optogenetic tool for fast and reversible removal of PRC1 from the spindle to the cell membrane, based on the previously designed improved light inducible dimer (iLID) system (Guntas et al., 2015). We attached PRC1 to the red fluorescent protein tgRFPt and the bacterial protein SspB, while the iLID, which contains the bacterial peptide SsrA and the light-oxygen-voltage (LOV2) domain, is bound to the cell membrane by a short peptide, CAAX. In this system, LOV2 adopts a conformation that allows dimerization of SsrA and SspB upon exposure to the blue light (**Fig. 1 A**). After cessation of exposure to the blue light, LOV2 adopts its initial conformation leading to decreased affinity of SsrA to SspB. Therefore, exposure to the blue light should induce translocation of PRC1 from the central region of the metaphase spindle, which we will refer to as the spindle midzone, to the cell membrane, whereas cessation of exposure to blue light should restore PRC1 localization on the spindle (**Fig. 1 A**).

To test our optogenetic approach, we used U2OS cells with stable expression of CENP-A-GFP, transient expression of PRC1-tgRFPt-SspB (henceforth opto-PRC1) and iLID-CAAX (henceforth opto cells; **Fig. 1 B**; **Video 1**). Endogenous PRC1 was depleted 90 ± 2% (all results are mean ± s.e.m.) by siRNA before addition of opto-PRC1 (**Fig. S1 A**). Before exposure to the blue light, opto-PRC1 had normal localization on the microtubule bundles in the spindle midzone (**Fig. 1 B**; 0:00 min), with the length of PRC1 streaks of 3.77 ± 0.08 μm (n=193 bundles, N=30 cells), consistent with that of endogenous and fluorescently labeled PRC1 in metaphase (Kajtez et al., 2016; Polak et al., 2017), though the total signal intensity of opto-PRC1 on the spindle was higher compared to endogenous PRC1 (**Fig. S1 B**). Addition of opto-PRC1 did not change the duration of metaphase, as inferred from the fraction of cells

that entered anaphase during image acquisition, which was similar in cells with endogenous PRC1 and cells treated with PRC1 siRNA and opto-PRC1 (79 ± 6 % N=37, and 71 ± 5 % N=72, respectively; p=0.4, Pearson's Chi-squared test; **Fig. S1 C**). Taken together, these data suggest that opto-PRC1 replaces the depleted endogenous PRC1.

Upon exposure to the blue light, opto-PRC1 signal on the spindle decreased and its signal on the membrane increased (**Fig. 1 B**; 0:20-20:00 min). After the blue light was switched off, opto-PRC1 returned to the spindle midzone (**Fig. 1 B**; 20:40-30:10 min). In control experiments without the blue light or without iLID (henceforth control), opto-PRC1 was not removed (**Fig. S1 D**). Thus, our optogenetic approach allows for acute and reversible control of PRC1 localization in metaphase.

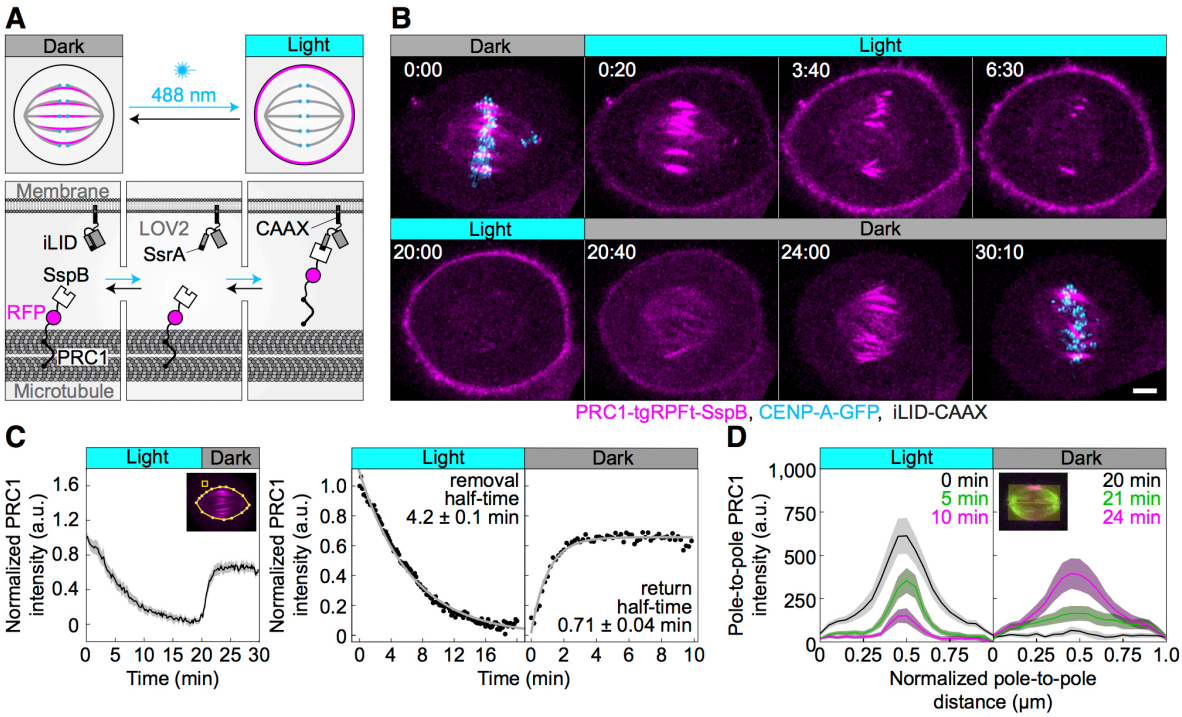


**Figure 1. Optogenetic reversible removal of PRC1 from the spindle in metaphase.**
(**A**) Schematic representation of the optogenetic system. PRC1 is fused with SspB and tgRFPt (opto-PRC1, see **Methods**). iLID, composed of photosensitive LOV2 domain and SsrA is tagged with CAAX sequence which mediates its binding to the cell membrane. Exposure to the blue light induces conformational change in LOV2 domain, enabling dimerization of SspB and SsrA, and thus translocation of PRC1 from the spindle to the cell membrane. After the blue light is turned off, LOV2 adopts its initial conformation, leading to decreased affinity of SspB for SsrA, and consequently dissociation of PRC1 from the membrane and its return to the spindle. (**B**) Time-lapse images of a metaphase spindle in a U2OS cell stably expressing CENP-A-GFP (cyan), depleted for endogenous PRC1, with transient expression of opto-PRC1 (magenta) and iLID-CAAX. Note that kinetochores are

shown only in the first and the last time frame in order to better visualize PRC1 removal. Images are maximum intensity projections of three z-planes, smoothed with 0.1-µm-radius Gaussian blur. Time; min:sec. Scale bar; 5 µm. (**C**) Normalized intensity of opto-PRC1 signal on the spindle (left panel) during its removal (0-20 min) and return (20-30 min). N=15 (see **Fig. S1 E** for individual cells). Scheme depicts the areas where opto-PRC1 intensity was measured: spindle (large polygon) and cytoplasm (small square). Exponential fit (gray lines in the right panel) on mean normalized opto-PRC1 spindle intensity (black points) during 20 min of removal (left) and 10 min of return (right). Formulas $y=A*e^{\tau*x}$ and $y=A*e^{\tau*x}+c$ were used for opto-PRC1 removal and return, respectively. Parameters for PRC1 removal: A=1.111, $\tau$=-0.00277 $s^{-1}$ (RSE=0.03), and return: A=-0.635, c=0.656, $\tau$=-0.01622 $s^{-1}$ (RSE=0.03). The half-time was calculated by ln0.5/$\tau$. (**D**) Pole-to-pole opto-PRC1 intensity during removal (left; N=14) and return (right; N=9) to the spindle. Mean and s.e.m are color-coded corresponding to the time when measured (upper right corners). Scheme depicts the area where opto-PRC1 intensity was measured (yellow) to obtain the mean intensity projection onto the pole-to-pole axis. Mean (thick lines); s.e.m. (shaded areas); N (number of cells).

To quantify the dynamics and spatial pattern of opto-PRC1 removal and return, we measured the intensity of opto-PRC1 on the metaphase spindle (**Fig. S1 E,F**). We found that 88 ± 3% of opto-PRC1 was removed after 20 min of exposure to the blue light with a half-time of 4.2 ± 0.1 min (**Fig. 1 C**). During the opto-PRC1 removal, there was simultaneous decrease in both signal intensity and length of the overlap region (**Fig. 1 D**, left; **Fig. S1 F**, top). The signal of the outermost midzone bundles typically lasted longer than of the inner ones (**Fig. 1 B**; 3:40-6:30). After the blue light was switched off, opto-PRC1 signal restored to 65 ± 1% of the initial intensity within 10 minutes, with return half-time being 0.71 ± 0.04 min (**Fig. 1 C**). During the opto-PRC1 return, it initially localized throughout the spindle, with gradual increase in intensity in the spindle midzone (**Fig. 1 D**, right; **Fig. S1 F**, bottom). Thus, PRC1 exhibits faster return to the spindle than removal from the overlap bundles, and shows preference towards overlap regions, which is evident within minutes.

**PRC1 removal during metaphase affects kinetochore positioning at the spindle equator and chromosome segregation fidelity in early anaphase**

To explore the effect of acute PRC1 removal on the forces acting on chromosomes in the metaphase spindle, we visualized chromosomes by using SiR-DNA (Lukinavicius et al., 2015). Surprisingly, we observed some chromosome extrusions outside the metaphase plate upon PRC1 removal. We quantified chromosome alignment by measuring the total

chromosome area and found an increase of 10% upon PRC1 removal (**Fig. 2 A,B**; **Video 2).** The increase of chromosome area suggests that chromosome alignment on the metaphase plate was disturbed.

To study the origin of the altered chromosome alignment, we focused on the forces acting on kinetochores by using cells expressing CENP-A-GFP (**Fig. 2 C**). We first tested to what extent PRC1 removal affects inter-kinetochore tension. Inter-kinetochore distance ($d_{KC}$, **Fig. 2 D**), a readout of inter-kinetochore tension (Waters et al., 1996), was reduced when opto-PRC1 was removed (**Fig. 2 E**; **Fig. S2 A**), whereas it did not change in control cells (**Fig. 2 E**). The inter-kinetochore distance of peripheral was similar to central kinetochores, both before and after PRC1 removal **(Fig. S2 A**). The mean inter-kinetochore distance after 20 min of exposure to the blue light (0.79 ± 0.01 μm) was closer to metaphase (0.87 ± 0.01 μm) than prometaphase (0.66 ± 0.01 μm) values (see **Methods**), suggesting that tension was not completely lost and that these changes were not due to kinetochore detachment from k-fibers (**Fig. S2 A**). In agreement with this, the fraction of cells that entered anaphase during image acquisition was similar in control and opto cells (71 ± 5 % N=72, and 60 ± 5 % N=93, respectively; p=0.1, Pearson's Chi-squared test; **Fig. S1 C**), indicating that PRC1 removal did not activate the spindle assembly checkpoint. After opto-PRC1 return to the spindle, inter-kinetochore distance increased, suggesting restoration of tension, though not to the original value (**Fig. 2 E**). These results suggest that PRC1 has a role in maintaining tension on sister kinetochores.

To quantify kinetochore alignment on the equatorial plane, we measured the distances of sister kinetochore midpoints from the equatorial plane ($d_{EQ}$, **Fig. 2 D**). Surprisingly, we observed that removal of opto-PRC1 increased the displacement of sister kinetochore pairs from the equatorial plane (**Fig. 2 C,F**; **Fig. S2 B,C**; **Video 3**). Interestingly, before opto-PRC1 removal >95% of kinetochore pairs were found within the region of PRC1 streaks, i.e., less than 2 μm away from the equatorial plane, whereas opto-PRC1 removal resulted in excursions of some kinetochore pairs far outside this region (**Fig. S2 B**). These displaced kinetochores upon opto-PRC1 removal had lower inter-kinetochore distance in comparison to non-displaced ones, suggesting that kinetochore displacement was related to a more severe reduction of tension (**Fig. 2 G**). On average, kinetochores remained displaced even after opto-PRC1 return (**Fig. 2 F**). We conclude that PRC1 has a role in keeping kinetochores in tight alignment on the metaphase plate.

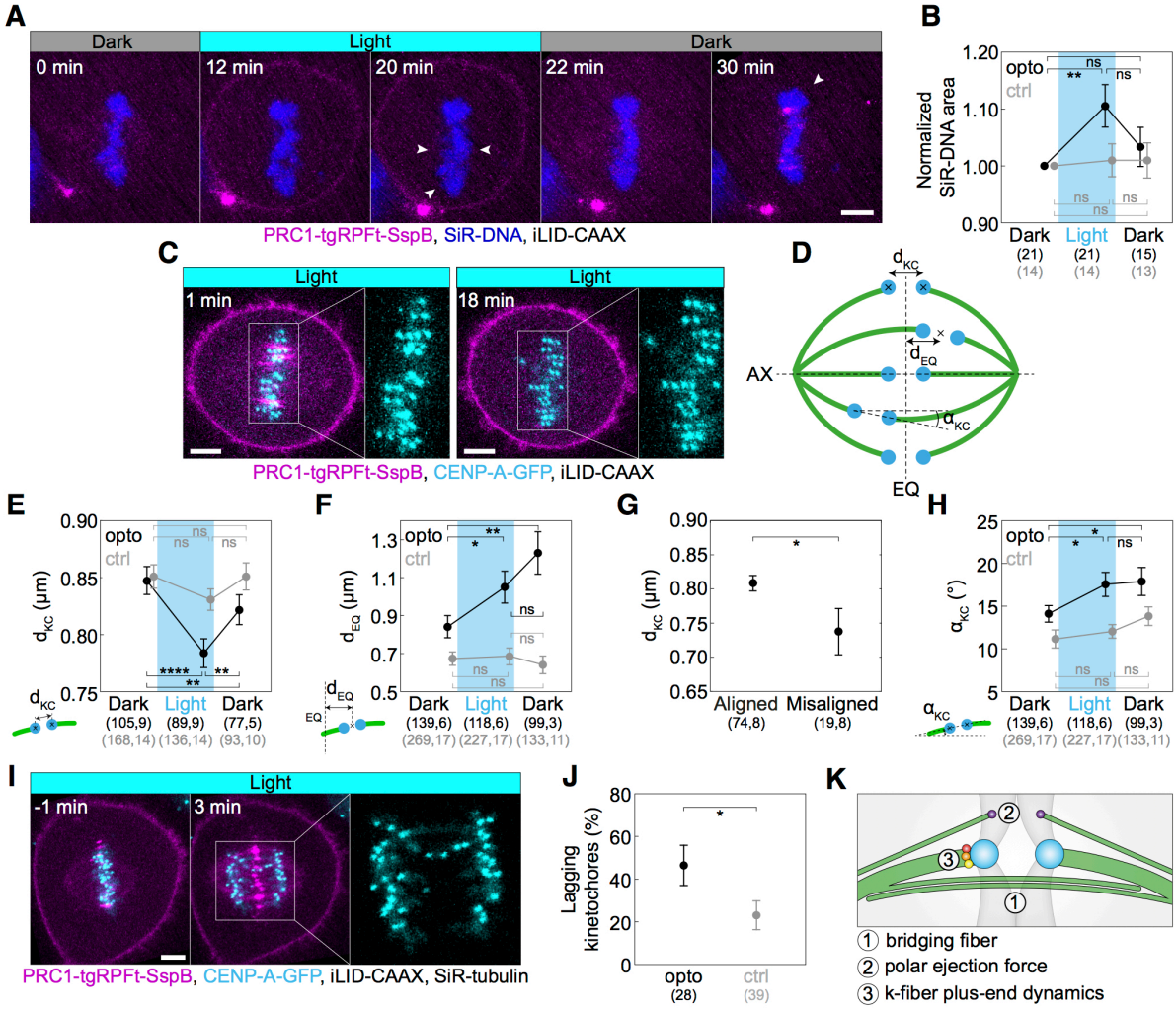


**Figure 2. Optogenetic removal of PRC1 disrupts kinetochore alignment on the metaphase plate and leads to lagging kinetochores in anaphase.**

(**A**) Time-lapse images of a U2OS cell depleted for endogenous PRC1, with transient expression of opto-PRC1 (magenta) and iLID-CAAX, and stained with SiR-DNA (blue). White arrowheads mark displaced chromosome mass. Scale bar; 2 µm. (**B**) Graph showing normalized SiR-DNA area in opto (black) and control (gray) cells before (0 min, Dark), at the end of continuous exposure (20 min, Light) and 10 min after cessation of exposure to the blue light (30 min, Dark), in U2OS cells without labeled tubulin and HeLa cells expressing GFP-tubulin. (**C**) Spindle in a U2OS cell stably expressing CENP-A-GFP (cyan) with transient expression of opto-PRC1 (magenta) and iLID-CAAX at the beginning (1 min, left) and at the end of continuous exposure to the blue light (18 min, right). Enlargements show kinetochores only. (**D**) Schematic of measured parameters. $d_{KC}$, inter-kinetochore distance; $d_{EQ}$, distance between sister kinetochore midpoint and equatorial plane (EQ); $\alpha_{KC}$, angle between sister kinetochore axis and spindle long axis (AX). (**E**) Measurements of $d_{KC}$. Legend as in **B**. (**F**) Measurements of $d_{EQ}$. Legend as in **B**. (**G**) $d_{KC}$ of aligned ($d_{EQ}$<2 µm) and misaligned ($d_{EQ}$=2.5 ± 0.2 µm) kinetochore pairs upon PRC1 removal. (**H**) Measurements of $\alpha_{KC}$. Legend as in **B**. (**I**) Time-lapse

images of a spindle in a U2OS cell as in **C,** stained with SiR-tubulin (not shown). Anaphase onset is at time 0 min. Lagging kinetochores can be seen at 3 min (middle). Enlargement shows kinetochores only. (**J**) Occurrence of lagging kinetochores in anaphase of opto (black) and control (gray) U2OS cells. (**K**) Schematic of three mechanisms that could be involved in kinetochore alignment. Cyan rectangles inside graphs indicate exposure to the blue light. Numbers and single numbers in brackets are measurements and cells, and cells, respectively. In **E, F, H** opto cells are without SiR-tubulin, and control cells include those with and without SiR-tubulin. All images are maximum intensity projections of three z-planes, smoothed with 0.5-pixel-radius Gaussian blur. Error bars; s.e.m. Scale bars; 5 µm. Statistical analysis; t-test (**B**, **E, F, G, H**), two-proportions z-test (**J**). p-value legend: < 0.0001 (****), 0.0001 to 0.001 (***), 0.001 to 0.01 (**), 0.01 to 0.05 (*), ≥ 0.05 (ns).

To investigate the influence of acute PRC1 removal on the orientation of sister kinetochores, we measured the angle between sister kinetochore axis and long spindle axis ($\alpha_{KC}$, **Fig. 2 D**). We observed that removal of opto-PRC1 increased the angle of sister kinetochore pairs (**Fig. 2 C,H**; **Fig. S2 C,D**). Interestingly, sister kinetochore pairs remained misoriented even after opto-PRC1 return (**Fig. 2 H**). The observed effects of PRC1 removal on inter-kinetochore distance, kinetochore alignment and orientation did not change when SiR-tubulin was added (compare **Fig. 2 E**,**F**,**H** without SiR-tubulin and **Fig. S2 A,B,D** including SiR-tubulin stained cells). Similarly, PRC1 bundles were misoriented upon PRC1 return (see **Methods**, **Fig. S2 E**). These results suggest that orientation of kinetochores is related to the orientation of PRC1 bundles. The orientations did not depend on the position in the metaphase spindle (**Fig. S2 F**). None of the effects were observed in control experiments (**Fig. 2 B,E,F,H**; **Fig. S2, A-E**). We conclude that PRC1 plays a role in maintaining kinetochore alignment and orientation within the metaphase plate.

To test to what extent the acute removal of PRC1 during metaphase affects chromosome segregation, we measured the frequency of lagging kinetochores. We found that lagging kinetochores occurred more frequently when opto-PRC1 was being removed than in control cells (**Fig. 2 I,J**; **Video 4**). Opto cells with lagging kinetochores did not show a wider metaphase plate but had a slightly decreased inter-kinetochore distance before anaphase in comparison with opto cells without lagging kinetochores (**Fig. S2 G)**. Moreover, as perturbation of the PRC1-CLASP1 interaction and the consequent absence of CLASP1 from the spindle midzone results in lagging chromosomes (Liu et al., 2009), we tested CLASP1 and found that it did not accumulate between segregating chromosomes in opto HeLa cells stably expressing EGFP-CLASP1 (**Fig. S2 H**). Thus, the observed higher occurrence of lagging

kinetochores could be attributed to changes in tension during metaphase, perturbed recruitment of CLASP1 to the spindle midzone by PRC1 during early anaphase, or a combination of both effects.

**Removal of PRC1 partially disassembles bridging fibers and affects spindle shape**

The observed effects of opto-PRC1 removal on kinetochore alignment and occurrence of lagging kinetochores could be attributed to 1) loss of microtubules in the bridging fibers, 2) disruption of polar ejection forces, and/or 3) disruption of localization of proteins that modulate the dynamics of k-fiber plus-ends (**Fig. 2 K**). Because PRC1 crosslinks microtubules within bridging fibers (Kajtez et al., 2016; Polak et al., 2017), we first tested to what extent PRC1 removal in metaphase affects the number of microtubules in the bridging fibers. We expect that removal of opto-PRC1 would result in reduction of bridging fibers (**Fig. 3 A**). In order to visualize microtubules both during PRC1 removal, when the blue light is turned on to activate the optogenetic system, and during return, when the blue light must be switched off, we used SiR-tubulin, a far-red tubulin dye excited by red light (Lukinavicius et al., 2014). Intensity profiles across the spindle midzone revealed that SiR-tubulin intensity maxima were lower upon PRC1 removal and increased after its return (**Fig. S3 A**; **Video 5).** Measurements of SiR-tubulin intensity between and lateral from sister kinetochores, following the approach from our previous study (Kajtez et al., 2016), showed impact of PRC1 removal specifically on bridging fibers (**Fig. 3, A-C**; **Video 5**). As an alternative to SiR-tubulin, which is a taxol-based dye that may affect microtubule dynamics (Lukinavicius et al., 2014) and marks only long-lived microtubules (David et al., 2019), we tested YFP-tubulin, but the excitation laser for YFP also activated the optogenetic system (Wang and Hahn, 2016) (**Fig. S1 G**).

Finally, we used tubulin-GFP to determine tubulin signal intensities of the bridging fibers and k-fiber tips upon acute removal of PRC1 (**Fig. 3 A,D,E**; **Fig. S3 B,C**; see **Methods**). In these cells opto-PRC1 was removed and returned to a similar extent as in cells with unlabeled tubulin (compare **Fig. 1 C** and **Fig. S 3D**). As k-fibers in HeLa cells contain roughly 17 microtubules (McEwen et al., 2001; Wendell et al., 1993), we have previously estimated the average number of microtubules in the bridging fiber to be 14, by calculating the ratio of bridging fiber intensity and sum of bridging fiber and k-fiber intensity (Kajtez et al., 2016). We used this as the initial number of microtubules in the bridging fiber. Upon

exposure to the blue light, tubulin signal intensity in the bridging fibers decreased ~2.5 fold, which corresponds to 5.6 ± 0.9 microtubules. Upon PRC1 return the intensity and thus number of microtubules remained low (**Fig. 3, D-F**; **Fig. S3 C**). Intensity at the position lateral from the k-fiber tips, as well as all parameters in control cells were unaltered (**Fig. 3 F,G**; **Fig. S3 C,E**). Thus, acute removal of PRC1 and its return change the number of microtubules in the bridging fibers. Since bridging fibers only partially disassembled, and Eg5/kinesin-5, which localizes in the bridging fibers (Kajtez et al., 2016; Mann and Wadsworth, 2018), was still detectable in these fibers after PRC1 siRNA (**Fig. S3 F**), we speculate that microtubule crosslinkers such as Eg5 crosslink the remaining microtubules in the bridge after acute PRC1 removal.

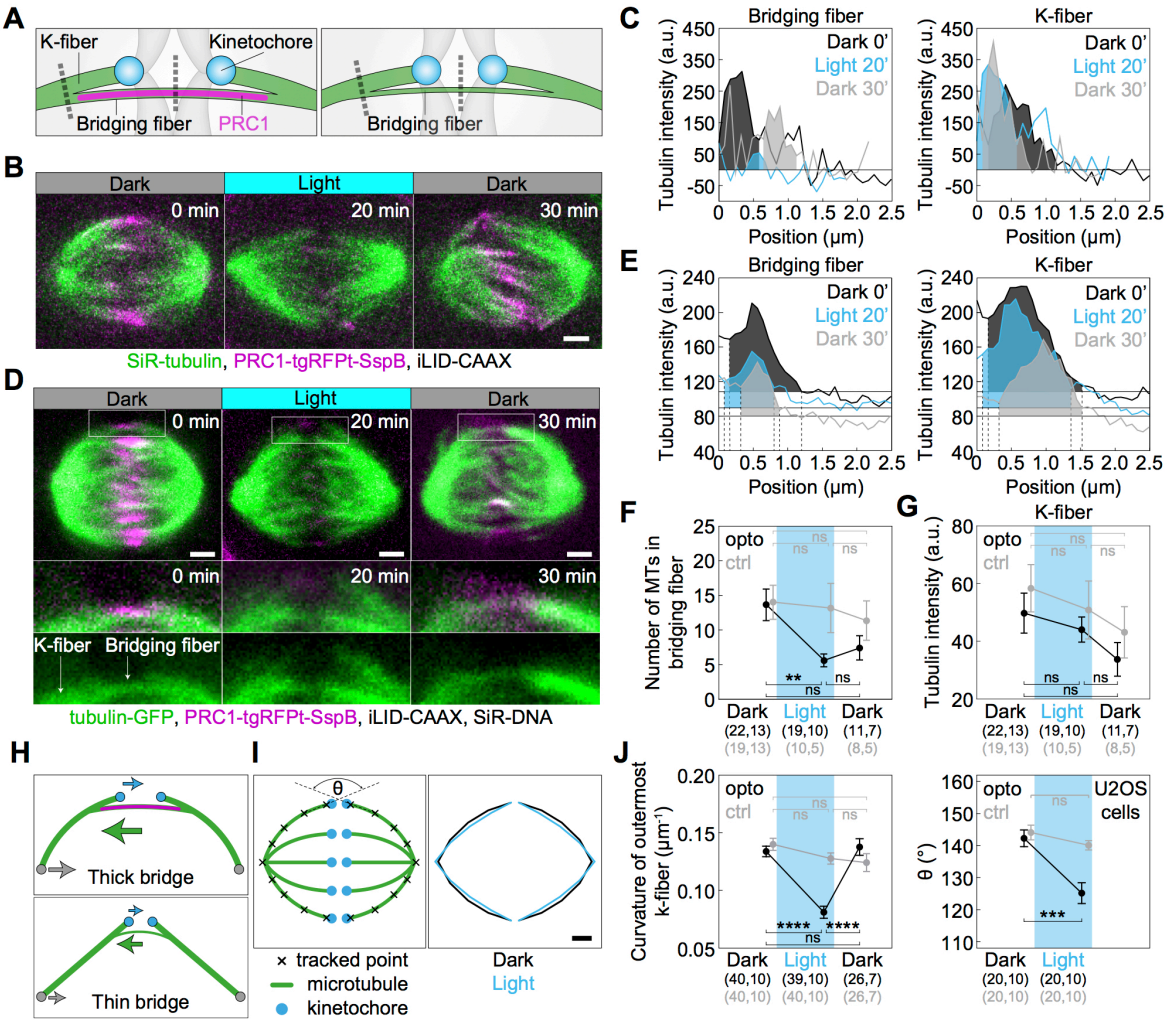


**Figure 3. Optogenetic removal of PRC1 reduces bridging fibers and straightens the spindle contour.**

(**A**) Schematic of PRC1 (magenta) removal from bridging fibers and positions where bridging fiber and k-fiber intensities were measured (dashed lines). (**B**) Spindle in a U2OS cell with stable

expression of CENP-A-GFP (not shown), depleted for endogenous PRC1, with transient expression of opto-PRC1 (magenta) and iLID-CAAX, and stained with SiR-tubulin (green), before exposure to the blue light (0 min, Dark), at the end of continuous exposure to the blue light (20 min, Light), and 10 min after cessation of exposure to the blue light (30 min, Dark). Images are a single z-plane smoothed with 0.5-pixel-radius Gaussian blur. (**C**) Background-corrected SiR-tubulin intensity profiles of the bridging fiber (left) and k-fiber (right) for cell shown in **B** (0 min, black; 20 min, cyan; 30 min, gray). (**D**) Spindle in a HeLa cell with stable expression of tubulin-GFP (green), depleted for endogenous PRC1, with transient expression of opto-PRC1 (magenta) and iLID-CAAX, and stained with SiR-DNA (not shown), before exposure to the blue light (0 min, Dark, left), at the end of continuous exposure to the blue light (20 min, Light, middle) and 10 min after cessation of exposure to the blue light (30 min, Light, right). Enlargements of the boxed region (middle: merge, bottom: GFP) are shown. Note that at 20 min opto-PRC1 is absent from the spindle. (**E**) Graphs showing tubulin-GFP intensity profiles of the bridging fiber (left) and k-fiber (right) (0 min, black; 20 min, cyan; 30 min, gray) for cell shown in **D**. Horizontal line marks the background signal, vertical dashed lines delimit the area (shaded) where signal was measured. (**F**) Number of microtubules in the bridging fiber in opto HeLa cells (i.e., where PRC1 was removed; black) and control (gray) in same time-points as in **D**. The bridging fiber intensity in control cells before exposure to the blue light is set to correspond to 14 microtubules (see **Fig. S3 C**). (**G**) Tubulin-GFP signal intensity laterally from k-fiber tip in opto (black) and control (gray) at time-points as in **D**. (**H**) Top: Schematic of force-balance in the spindle where compression in the bridging fiber (green arrow) balances compression at the poles (gray arrow) and tension at kinetochores (cyan arrow). Bottom: Upon PRC1 removal, reduction of number of microtubules in the bridging fiber is expected to reduce compression in the bridging fiber and at the poles, leading to k-fiber straightening. (**I**) Outermost k-fiber contours (right) in opto U2OS cells before (black, Dark) and at the end of continuous exposure to the blue light (cyan, Light) plotted by connecting mean positions of all tracked points. Scheme (left) depicts how contours were tracked. θ; angle between outermost k-fibers (**J**) Curvature of the outermost k-fibers (left) in opto (black) and control (gray) U2OS cells in same time-points as in **B**. Angle between outermost k-fibers (right) in opto (black) and control (gray) U2OS cells at first two time-points as in **B**. Cyan rectangles inside graphs indicate exposure to the blue light. Numbers in brackets; number of measurements and cells, respectively. Error bars; s.e.m. Scale bars; 2 μm. Statistical analysis; t-test. p-value legend as in **Fig. 2**.

We next asked how the loss of microtubules in the bridging fiber affects the force balance in the spindle. According to our previously proposed theoretical model (Kajtez et al., 2016; Tolic and Pavin, 2016), spindles with thicker bridging fibers are expected to have a curved shape, whilst spindles with thinner bridging fibers are expected to have a more diamond-like shape (Kajtez et al., 2016) (**Fig. 3 H**). To test this prediction, we tracked the

pole-to-pole contour of the outermost k-fibers, and found that removal of PRC1 caused a decrease in the curvature of the spindle and the angle between outermost sister k-fibers (**Fig. 3 I,J**; **Fig. S3 G**), while spindle length and width remained constant (**Fig. S3 H**). Therefore, the acute removal of PRC1 reduces the number of microtubules in the bridging fibers and makes the spindle diamond-shaped, corroborating a role of the bridging fiber in the force balance of the metaphase spindle.

**Removal of PRC1 affects the localization of proteins in the bridging fiber, but not on chromosomes and k-fibers**

Our results suggest that the kinetochore misalignment and increased occurrence of lagging kinetochores upon PRC1 removal are due to loss of microtubules in the bridging fibers. Alternatively, these effects may be caused by disruption of polar ejection forces (**Fig. 2 K**), which are modulated by Kif4A/kinesin-4 (Stumpff et al., 2012), a binding partner of PRC1. To test this possibility, we used U2OS cells silenced for endogenous PRC1 with transient expression of GFP-Kif4A, opto-PRC1 and iLID-CAAX (**Fig. 4 A**). In metaphase, Kif4A localized on chromosomes, while in anaphase on chromosomes and spindle midzone, as previously shown (Gruneberg et al., 2006; Kurasawa et al., 2004; Zhu and Jiang, 2005) (**Fig. 4 A**; **Fig. S4 A,B**). Removal of opto-PRC1 from the spindle had no effect on Kif4A signal on the chromosomes in metaphase (**Fig. 4 A**; **Fig. S4 C)**. This result is consistent with previous reports that Kif4A does not directly interact with PRC1 before late mitosis (Gruneberg et al., 2006; Kurasawa et al., 2004; Zhu and Jiang, 2005). Similarly, Kif4A remained on the chromosomes, and was removed from bridging fibers after long-term removal of PRC1 by siRNA (**Fig. 4 B**, **Table 1**). Thus, metaphase localization of Kif4A on chromosomes does not depend on PRC1, suggesting that the observed changes in kinetochore alignment are not caused by disruption of polar ejection forces. In early anaphase, the amount of Kif4A on segregated chromosomes was similar in opto and control cells (**Fig. S4 D)**, indicating that increased occurrence of lagging kinetochores was not due to perturbed polar ejection forces or defects in chromosome architecture/condensation. Thus, we favor the interpretation that kinetochore misalignment and increase in lagging kinetochores upon PRC1 removal are caused by disruption of bridging fibers.

Another potential origin of kinetochore misalignment and increased occurrence of lagging kinetochores could be disrupted localization of plus-end proteins upon optogenetic

PRC1 removal (**Fig. 2 K**). To investigate this possibility, we analyzed the localization of CLASP1, Kif18A, and CENP-E, previously shown to regulate microtubule dynamics (Al-Bassam et al., 2010; Barisic et al., 2014; Gudimchuk et al., 2013; Maiato et al., 2003; Mayr et al., 2007; Schaar et al., 1997; Stumpff et al., 2008; Stumpff et al., 2012; Yu et al., 2016), on the plus-ends of k-fibers before and after PRC1 removal in metaphase. CLASP1, Kif18A, and CENP-E were visible on plus-ends of k-fibers before and after acute removal of PRC1 (**Fig. 4 A**; **Table 1**), as well as after long-term removal of PRC1 by siRNA (**Fig. 4 B**; **Table 1**). In contrast to the localization on the k-fiber, the localization of Kif18A in the bridge was perturbed by both acute and long-term PRC1 removal (**Fig. 4 A,B**; see **Table 1** for all proteins). Therefore, we propose that kinetochore misalignment and increase in lagging kinetochores upon PRC1 removal are not caused by removal of proteins that regulate microtubule dynamics from the k-fiber plus ends.

Finally, we set out to examine how the optogenetic removal of PRC1 affects localization of its binding partner specifically localized in the spindle midzone, MKLP1/kinesin-6 (Gruneberg et al., 2006; Kurasawa et al., 2004), (**Fig. 4A**; **Fig. S4 E**). In metaphase, MKLP1-GFP co-localized with opto-PRC1 in the spindle midzone, which was also the case for endogenous MKLP1 and PRC1 in unlabeled cells (**Fig. S4 F,G**). Removal of opto-PRC1 from the spindle caused MKLP1-GFP signal disappearance from the spindle (**Fig. 4 A**; **Fig. S4 G**). However, MKLP1 signal was undetectable on the membrane, consistent with MKLP1 and PRC1 not interacting before late mitosis (Gruneberg et al., 2006; Kurasawa et al., 2004) (**Fig. S4 G**). Similarly, MKLP1 was removed from the spindle after long-term removal of PRC1 by siRNA (**Fig. 4 B**; **Table 1**). Upon opto-PRC1 return to the spindle, we observed MKLP1-GFP signal reappearance in the overlap bundles (**Fig. 4 A**; **Fig. S4 G**). These results suggest that PRC1 is required to localize MKLP1 to overlap bundles in metaphase.

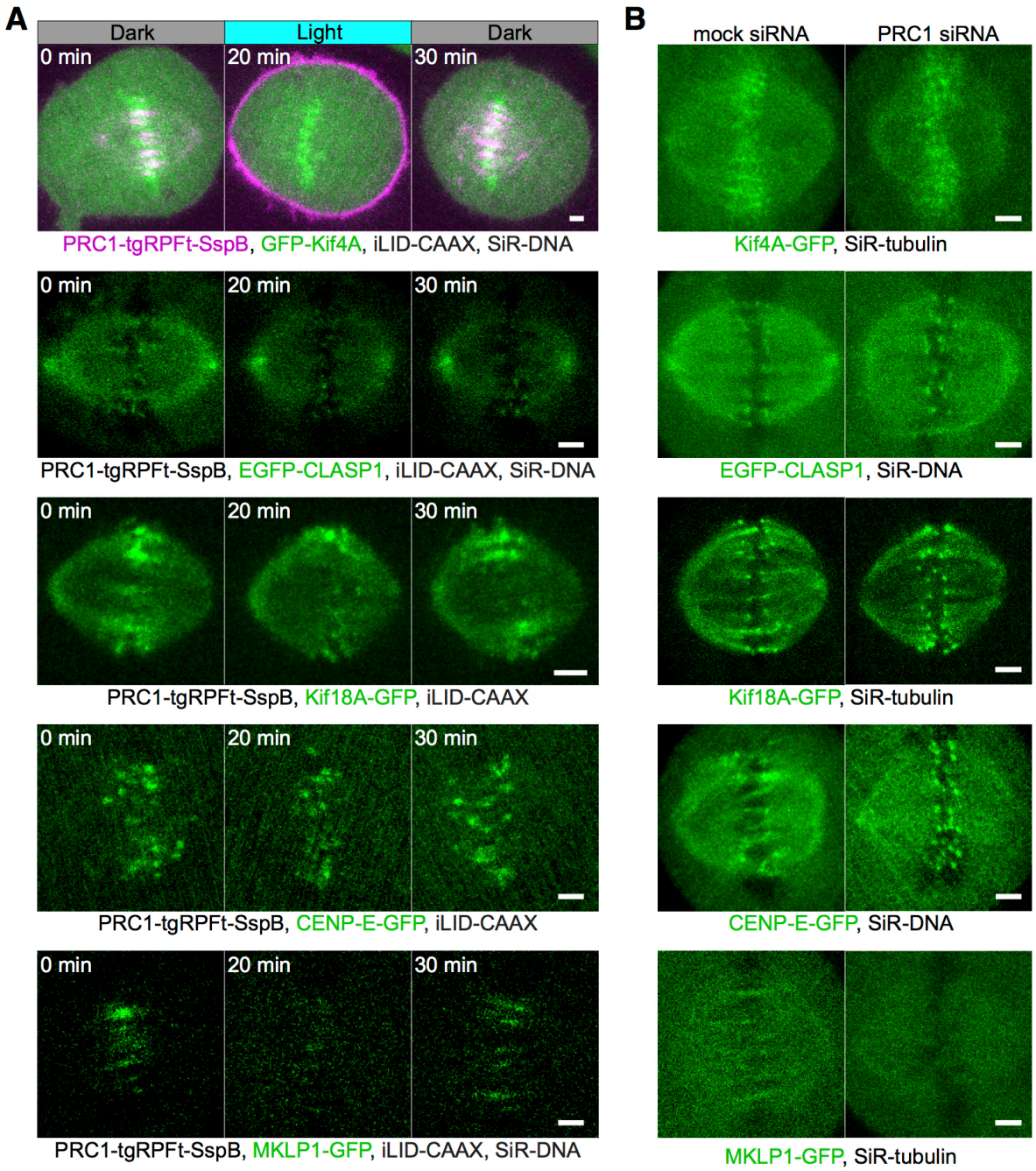


**Figure 4. Localization of Kif4A, CLASP1, Kif18A, CENP-E and MKLP1 after acute removal and long-term depletion of PRC1**

(**A**) Time-lapse images of: unlabeled U2OS cell with transient expression of opto-PRC1 (magenta), iLID-CAAX and GFP-Kif4A (green), and stained with SiR-DNA (not shown) (first row); HeLa cell with stable expression of EGFP-CLASP1 (green) with transient expression of opto-PRC1 and iLID-CAAX, and stained with SiR-DNA (second row); unlabeled U2OS cell with transient expression of opto-PRC1, iLID-CAAX and EGFP-Kif18A (green) (third row); unlabeled U2OS cell with transient expression of opto-PRC1, iLID-CAAX and GFP-CENP-E (green) (fourth row); HeLa BAC cell stably expressing MKLP1-GFP (green) and with transient expression of opto-PRC1 and iLID-CAAX, and

stained with SiR-DNA (fifth row). All time points are before (0 min, Dark), at the end of continuous exposure (20 min, Light) and 10 min after cessation of exposure to the blue light (30 min, Dark). (**B**) Images of mock (left column) and PRC1 siRNA treated (right column): HeLa BAC cell expressing Kif4A-GFP (green) stained with SiR-tubulin (first row); HeLa cell stably expressing EGFP-CLASP1 (green) stained with SiR-DNA (second row); HeLa BAC cell expressing Kif18A-GFP (green) (third row); HeLa BAC cell expressing CENP-E-GFP (green) stained with SiR-DNA (fourth row); HeLa BAC cell expressing MKLP1-GFP (green) stained with SiR-tubulin (fifth row). All images are maximum intensity projections of 2-3 z-planes, smoothed with 0.5-pixel-radius Gaussian blur. Scale bars; 2 µm.

**Table 1. Localization of proteins in the bridging fiber and at kinetochores after acute and long-term removal of PRC1.** For long-term depletion, p-values for localization in the bridging fiber - Kif4A: 0.043; MKLP1: $8*10^{-6}$; CLASP1: 0.113; Kif18A: 0.033. Statistics: Pearson's Chi-squared test.
In acute removal protein is considered present if at least 83% of cells had it in the bridge and absent if it was undetectable in at least 66% of inspected cells.
Numbers in brackets; number of cells. Legend: + present, - absent, +/- unclear.
*in the case of Kif4A kinetochore (KC) localization includes chromosome arms.

| | **Acute removal** | | | | **Long-term depletion** | | | |
|---|---|---|---|---|---|---|---|---|
| | Dark (0 min) | | Light (20 min) | | mock | | siRNA | |
| | Bridge | KC | Bridge | KC | Bridge | KC | Bridge | KC |
| Kif4A* | + (6) | + (6) | +/- (6) | + (6) | + (10) | + (10) | - (16) | + (16) |
| CLASP-1 | +/- (5) | + (5) | +/- (5) | + (5) | + (15) | + (15) | + (8) | + (8) |
| Kif18A | + (6) | + (6) | - (6) | + (6) | + (18) | + (18) | - (8) | + (8) |
| CENP-E | +/- (5) | + (5) | +/- (5) | + (5) | +/- (6) | + (6) | +/- (10) | + (10) |
| MKLP-1 | + (6) | - (6) | - (6) | - (6) | + (19) | - (19) | - (9) | - (9) |

## Acute and long-term removal of PRC1 result in partially different effect on spindle microtubules and kinetochores

Previous reports have shown that acute rapamycin-dependent protein translocation and long-term depletion by siRNA can yield different and even opposite phenotypes (Cheeseman

et al., 2013; Wordeman et al., 2016). To explore to what extent acute optogenetic removal of PRC1 affects the spindle differently than long-term depletion by siRNA, we compared the phenotypes obtained by these two approaches (**Table 2**). Similarly as acute removal, long-term depletion of PRC1 decreased the number of microtubules in the bridging fiber and caused straightening of outermost k-fibers, whereas spindle length and width was unchanged (**Fig. S5, A-D**). However, the effects of acute removal of PRC1 were more severe than those of siRNA (**Table 2**). The two methods decreased the inter-kinetochore distance to a similar extent (**Table 2**; **Fig. S5 E**), even though unlike acute removal, long-term removal reduced the fraction of cells that entered anaphase (35 ± 8 % N=37, and 79 ± 6 % N=37, for PRC1 siRNA treated and untreated, respectively; p=0.046, Pearson's Chi-squared test; **Fig. S1 C**). Strikingly, in contrast to acute removal, the long-term depletion did not cause kinetochore misalignment or misorientation (**Fig. S5 F,G**). Finally, both long-term and acute PRC1 reduction increased the frequency of lagging kinetochores during early anaphase (**Fig. S5 H**).

**Table 2. Comparison of effects of acute optogenetic removal of PRC1 and long-term depletion by siRNA.** All values are given as mean ± s.e.m. The numbers in the brackets denote the number of measurements and cells, respectively; a single number is the number of cells. Symbols (arrows and equal signs) denote trend of change of parameters; equal sign means no change; longer arrow marks stronger effect.

*calculated from our previous study (Polak et al., 2017)

[#]consistent with our previous studies (Kajtez et al., 2016; Polak et al., 2017)

| **Parameter** | **Acute removal** | | | | **Long-term depletion** | | | |
|---|---|---|---|---|---|---|---|---|
| | 0 min | 20 min | p-value | | untreated | siRNA | p-value | |
| **N (microtubules) in the bridging fiber** | 14 ± 2 (22,13) | 5.6 ± 0.9 (19,10) | 0.0038 | ↓ | 14 ± 1 (16, 9)* | 10 ± 1 (21,6)* | 0.048 | ↓ |
| **Curvature** ($\mu m^{-1}$) | 0.134 ± 0.004 (40, 10) | 0.081 ± 0.005 (39, 10) | $6*10^{-11}$ | ↓ | 0.137 ± 0.006 (20, 5) | 0.108 ± 0.004 (52,13) | 0.0014 | ↓ |
| **θ** (°) | 142 ± 3 (20, 10) | 125 ± 3 (20, 10) | $2*10^{-4}$ | ↓ | 145 ± 3 (10, 5) | 137 ± 2 (26, 13) | 0.051 | = |

| | | | | | | | | |
|---|---|---|---|---|---|---|---|---|
| **$d_{KC}$** (µm) | 0.87 ± 0.01 (226,18) | 0.79 ± 0.01 (186, 18) | $1*10^{-8}$ | ↓ | 0.85 ± 0.01 (75, 8)# | 0.780 ± 0.008 (202, 17)# | $4*10^{-6}$ | ↓ |
| **$d_{EQ}$** (µm) | 0.78 ± 0.04 (290, 17) | 0.94 ± 0.05 (240, 16) | 0.035 | ↑ | 0.69 ± 0.05 (107, 8) | 0.69 ± 0.03 (333, 17) | 0.64 | = |
| **$d_{EQ}$>2 µm** (%) | 4.1 ± 1.2 (290, 17) | 8.3 ± 1.8 (240, 16) | 0.043 | ↑ | 3.3 ± 1.0 (107, 8) | 0.9 ± 0.9 (333, 17) | 0.33 | = |
| **$\alpha_{KC}$** (°) | 13.8 ± 0.7 (290, 17) | 18.4 ± 1.0 (240, 16) | 0.0013 | ↑ | 13.3 ± 1.0 (107, 8) | 10.3 ± 0.7 (333, 17) | $1*10^{-4}$ | ↓ |
| **$\alpha_{KC}$>35°** (%) | 6.2 ± 1.4 (290, 17) | 12.1 ± 2.1 (240, 16) | 0.018 | ↑ | 4.7 ± 2.0 (107, 8) | 3.6 ± 1.0 (333, 17) | 0.83 | = |
| **Lagging kinetochores** (%) | 23 ± 7 (39) control | 46 ± 9 (28) opto | 0.044 | ↑ | 5 ± 4 (37) | 40 ± 11 (20) | 0.0036 | ↑ |

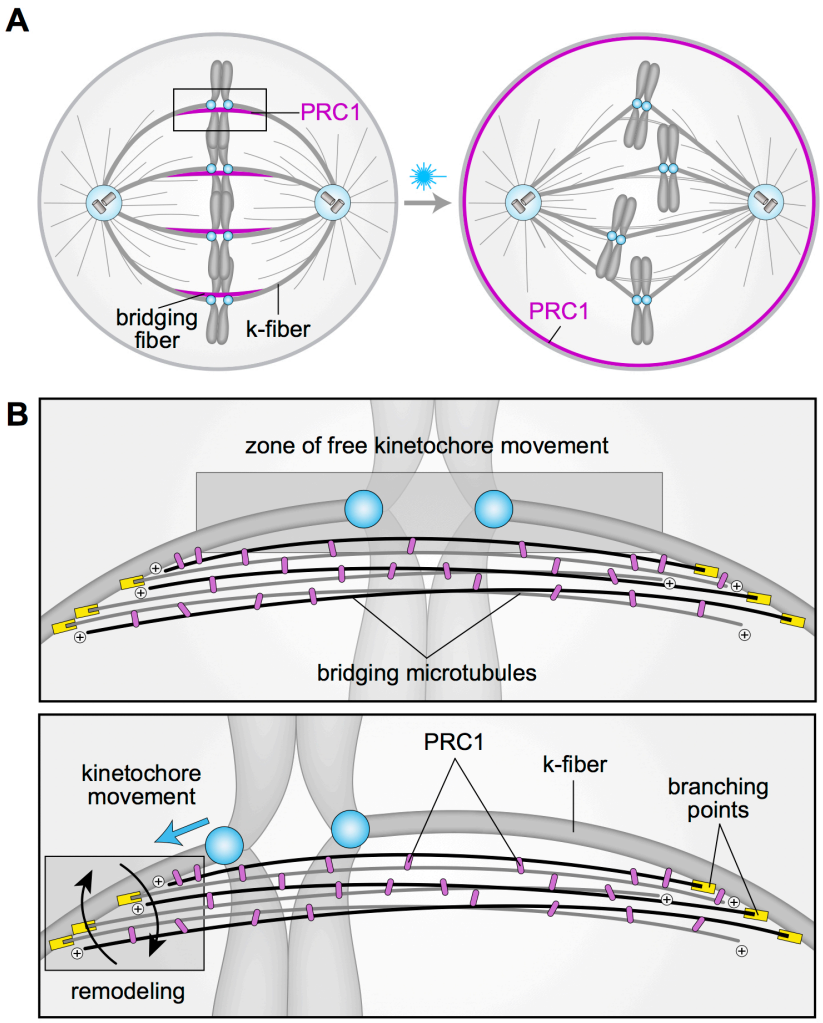

**Figure 5. Model for PRC1 function in spindle mechanics and chromosome alignment in metaphase.**

(**A**) In control cells (left), PRC1 (magenta) crosslinks antiparallel regions within bridging fibers and between bridging and kinetochore fibers. Upon acute PRC1 removal from the spindle to the cell membrane (right), bridging fibers are largely disassembled and the loss of PRC1-mediated crosslinks between k-fibers and bridging microtubules leads to chromosome misalignment and misorientation, as well as reduction of inter-kinetochore tension. Force balance of the entire spindle is altered, which is reflected in the straightening of k-fibers and a diamond-like shape of the spindle, indicating that the mechanical coupling between bridging and k-fibers is crucial for spindle mechanics and maintenance of spindle shape.

(**B**) Model for regulation of chromosome alignment by bridging fibers. Enlargement of the boxed region from **A** is shown. PRC1 (magenta) crosslinks antiparallel microtubules within the bridging fiber, as well as antiparallel regions between k-fibers and bridging microtubules. Kinetochore movement, driven by k-fiber polymerization and depolymerization, is unimpeded within the region where k-fibers are separated from bridging microtubules (top, gray rectangle). Kinetochore movement beyond that region (bottom, blue arrow) requires remodeling of the interactions between bridging microtubules and k-fibers, which may progressively slow down the kinetochores. Thus, the bridging fiber promotes chromosome alignment by buffering kinetochore movements.

## DISCUSSION

We developed an optogenetic approach that offers acute light-controlled removal of proteins from a normally formed spindle at a precise phase of mitosis. The main advantages of this approach over chemically-induced protein translocation (Cheeseman et al., 2013; Haruki et al., 2008; Robinson et al., 2010; Wordeman et al., 2016) are its reversibility, allowing the protein to return to its initial location within about a minute, and applicability to individual cells. Unlike previous optogenetic approaches (Fielmich et al., 2018; Okumura et al., 2018; van Haren et al., 2018; Yang et al., 2013; Zhang et al., 2017), this method allows for global loss-of-function of full-length spindle proteins, relying on simple protein tagging rather than domain splitting, with no need of chromophore addition. Moreover, this method may be implemented with other optical perturbations (Milas et al., 2018) and used as "*in vivo* pull-down" for probing protein-protein interactions in different phases of the cell cycle. However, this approach depends on high turnover of the protein in comparison with the time scale of interest.

Electron microscopy studies have shown that minus ends of microtubules that form overlap bundles are embedded in k-fibers and that the majority of their antiparallel regions is positioned in the central part of the bundle (Mastronarde et al., 1993; O'Toole et al., 2019). We observed a simultaneous decrease in both width and height of PRC1 signal intensity peak during optogenetic removal of PRC1, which may be due to fewer antiparallel regions being positioned laterally than in the central part of the bridging fiber, or destabilization of microtubule plus-ends leading to depolymerization, directly by PRC1 or indirectly by CLASP1 removal (Kellogg et al., 2016; Liu et al., 2009). A different spatial pattern of PRC1 return to the spindle, where we observed that PRC1 first binds all along the spindle and then gradually accumulates in the overlap regions of the bridging fibers, suggests that PRC1 has higher unbinding rate outside than within the overlap bundles in the spindle. This result is consistent with PRC1 having a life-time of several seconds on single microtubules and a 10-fold preference for overlap regions *in vitro* (Subramanian et al., 2010). The faster PRC1 return to the spindle in comparison with its removal may be due to the higher affinity difference between PRC1 binding to the spindle and to the membrane when the system is inactive. PRC1 did not completely return to the spindle, which could be a result of an incomplete recovery of microtubules in the bridging fibers, yet PRC1 recovered to a larger extent than microtubules in the bridging fibers, presumably because there are sufficient binding sites for PRC1 even on a bridging fiber with fewer microtubules. Nevertheless, the recovery of both PRC1 and microtubules could be more complete after a longer time period.

As bridging fibers link sister k-fibers, reduction of microtubules in the bridging fibers, leading to a decrease in compressive forces within the bridging fibers, can account for the observed straightening of outermost k-fibers, which made the spindle less round and more diamond-like, as well as for reduction of inter-kinetochore tension, consistent with our theoretical model (Kajtez et al., 2016). This reduction in inter-kinetochore tension was due to partial disintegration of bridging fibers rather than changes in k-fiber structure or detachment of kinetochores from k-fibers, given that the tubulin signal intensity in k-fibers did not change, and the inter-kinetochore distance upon PRC1 removal was closer to metaphase than prometaphase values. Together with the finding that PRC1 removal partially disassembles bridging fibers, this result provides support for a role of bridging fibers in balancing tension on kinetochores (Kajtez et al., 2016; Milas and Tolic, 2016), similar to local load-bearing near kinetochores by NuMA (Elting et al., 2017).

Surprisingly, acute removal of opto-PRC1 affected the alignment and orientation of sister kinetochores with respect to the equatorial plane. The observed misalignment of

kinetochores could be caused by reduction of polar ejection forces (Rieder et al., 1986; Rieder and Salmon, 1994). However, we find this scenario unlikely because the chromosome localization of the chromokinesin Kif4A, which interacts with PRC1, was unchanged after acute removal of opto-PRC1 in metaphase. It is also unlikely that the kinetochore misalignment was due to disrupted localization of plus-end proteins because CLASP1, Kif18A, and CENP-E remained localized on plus-ends of k-fibers upon acute PRC1 removal. Although we cannot exclude the possibility that other plus-end proteins were mislocalized, our data suggest that the perturbed alignment and orientation of kinetochores are due to disruption of bridging fibers.

Though the average effect on kinetochore alignment was modest, 10-15% of inspected kinetochore pairs were severely misaligned, undergoing displacement larger than 2 µm away from the equatorial plane. Interestingly, these kinetochores had a decreased inter-kinetochore distance compared to kinetochores that remained aligned. The misaligned kinetochores were found in the inner part of the spindle, where PRC1 signal disappeared faster than on the outer part, which may indicate that the inner bridging fibers were more severely affected. Thus, our interpretation is that the misaligned kinetochores were displaced due to especially strong reduction of their bridging fibers.

The changes in kinetochore positioning and orientation did not revert to the initial values within 10 min of PRC1 return possibly due to incomplete recovery and misorientation of bridging fibers. Thus, bridging fibers set the region in which bi-oriented kinetochores are positioned and serve as a structural support that keeps the sister kinetochore axis aligned with the pole-to-pole axis.

The presence of MKLP1 on the spindle was dependent on PRC1, yet MKLP1 was not translocated to the cell membrane together with PRC1. It could be that MKLP1 binds rather weakly to PRC1 in metaphase and/or that the absence of PRC1 decreases its affinity for microtubules. In addition, the ability of MKLP1 to bind along scaffold of antiparallel overlaps could depend on the role of PRC1 in dictating 35-nm-inter-microtubule spacing, proposed to be important to enable localization of specific proteins within these structures (Kellogg et al., 2016; Subramanian et al., 2010).

We found differences in phenotypes upon acute PRC1 removal from the spindle by optogenetics and the long-term PRC1 depletion by siRNA. These differences are hard to explain by different levels of PRC1 on the spindle as both methods decreased PRC1 by ~90%. It is also unlikely that the differences are caused by the interaction of the membrane-translocated PRC1 with astral microtubules because of the uniform PRC1 signal on the

membrane, fast return to the spindle, and no change in spindle positioning. Therefore, the generally weaker effects of siRNA in comparison with the acute optogenetic removal are most likely due to compensatory mechanisms being triggered during long-term depletion.

By overcoming temporal limitations of siRNA, our work reveals an unexpected role of PRC1 and the corresponding bridging fibers in kinetochore alignment on the metaphase spindle. We propose a model in which the movement of bi-oriented kinetochores along the pole-to-pole axis is regulated by the interactions between k-fibers and bridging fibers (**Fig. 5**). These interactions are mediated by PRC1 and probably also by other microtubule crosslinkers. In our model, kinetochores move, driven by k-fiber polymerization and depolymerization, in an unrestrained manner around the spindle equatorial plane within the region where k-fibers do not interact with bridging microtubules. Kinetochore movement beyond that region requires remodeling of these interactions, which may impede the movement. Our findings that kinetochores normally move within the region of PRC1 streaks, whereas they make excursions beyond that region upon PRC1 removal, support this model. Thus, the bridging fiber promotes chromosome alignment by buffering movements of bi-oriented kinetochores via its PRC1-mediated crosslinks to sister k-fibers.

## Methods

**Cell lines.** Experiments were performed using: unlabeled human osteosarcoma U2OS cell line and U2OS cell line stably expressing CENP-A-GFP, used in our previous work (Vukusic et al., 2017), which was a gift from Marin Barišić and Helder Maiato (Institute for Molecular Cell Biology, University of Porto, Portugal); HeLa-Kyoto BAC lines stably expressing MKLP1-GFP, Kif4A-GFP, Kif18A-GFP and CENP-E-GFP were a courtesy of Ina Poser and Tony Hyman (MPI-CBG, Dresden, Germany); unlabeled HeLa-TDS cells from the High-Throughput Technology Development Studio (MPI-CBG, Dresden); HeLa-TDS cells, permanently transfected with pEGFP-α-tubulin, used in our previous work (Kajtez et al., 2016); HeLa cells stably expressing YFP-tubulin, a courtesy of Lars Jansen (University of Oxford, United Kingdom); HeLa cells permanently transfected with EGFP-CLASP1, which was a gift from Helder Maiato (Institute for Molecular Cell Biology, University of Porto, Portugal). Cells were grown in flasks in Dulbecco's Modified Eagle's Medium (DMEM; Lonza, Basel, Switzerland) with 1 g/L D-glucose, L-glutamine, and pyruvate, supplemented with 10% of heat-inactivated Fetal Bovine Serum (FBS; Sigma Aldrich, St. Louis, MO, USA),

100 IU/mL penicillin and 100 mg/mL streptomycin solution (Lonza). For cell lines with stable expression of fluorescently labeled proteins, 50 µg/mL geneticin (Life Technologies, Waltham, MA, USA) was added. Cells were kept at 37°C and 5% $CO_2$ in a Galaxy 170 R humidified incubator (Eppendorf, Hamburg, Germany). All used cell lines were confirmed to be mycoplasma free by using MycoAlert Mycoplasma Detection Kit (Lonza).

**Plasmids.** To make PRC1-tgRFPt-SspB WT (opto-PRC1) plasmid, PRC1 fragment was amplified from His6-PRC1 plasmid (Addgene number: 69111) (Nixon et al., 2015) using the primers GCTAGAATTGACCGGATGAGGAGAAGTGAGGTGCTG (FWD) and CATGGTGGCGACCGGTAAATTCGAAGCTTGAGCTCGAGATCTGAGGGACTGGAT GTTGGTTGAATTGAGG (REV) and inserted into plasmid tgRFPt-SspB WT (Addgene number: 60415) (Guntas et al., 2015) using *AgeI* restriction site. This step was performed using commercially available *In-Fusion HD Cloning Kit* (Clontech, Mountain View, CA, USA). The produced plasmid expresses PRC1 tagged with tgRFPt and SspB at the C-terminus. Plasmid iLID-CAAX was purchased (Addgene number: 85680) (O'Neill et al., 2016). Plasmids pEGFP-C1Kif4a-sires and EGFP-Kif18A were a gift from Jason Stumpff (University of Vermont, Burlington, VT, USA) (Stumpff et al., 2008; Stumpff et al., 2012). Plasmid GFP-CENP-E was a gift from Marin Barišić (Danish Cancer Society Research Center, Copenhagen, Denmark).

**Sample preparation.** For depletion of endogenous PRC1 before opto experiments, cells were transfected 72 h (U2OS cells) or 24 h (HeLa cells) prior to imaging with 25 µL of 20 µM *Accell PRC1 siRNA* (A-019491-15-0020, Dharmacon, Lafayette, CO, USA) targeting 3' UTR of PRC1 mRNA. A day prior to imaging, siRNA treated cells were transfected with corresponding plasmids in following amounts: 0.3 µg of iLID-CAAX, 5.5 µg PRC1-tgRFPt-SspB-WT, 0.5 µg pEGFP-C1Kif4a-sires, 1 µg EGFP-Kif18A and 1 µg GFP-CENP-E. In HeLa BAC lines, 24 h prior to imaging, mock experiments cells were transfected with 100 nM *Accell Non-targeting Pool* (D-001910-10-05, Dharmacon), whilst PRC1 siRNA treated with 100 nM *Accell PRC1 siRNA* (Dharmacon). All transfections were performed using Nucleofector Kit R with the Nucleofector 2b Device (Lonza) using X-001 program for U2OS and O-005 (high viability) program for HeLa cells. Following transfection, the cells were seeded on 35-mm glass coverslip uncoated dishes with 0.17-mm (1.5 coverglass) glass thickness (MatTek Corporation, Ashland, MA, USA) in 1.5 mL DMEM medium with appropriate supplements. To visualize microtubules, cells were stained with silicon rhodamine (SiR)-tubulin (Lukinavicius et al., 2014) (Spirochrome AG, Stein am Rhein, Switzerland), a

far-red tubulin dye, at a concentration of 50 nM 12-16 h prior to imaging. To prevent dye efflux, verapamil, a broad-spectrum efflux-pump inhibitor (Spirochrome Ltd.), was added in U2OS cells at a concentration of 1 μM. To visualize chromosomes and determine the phase of the mitosis, 20 min prior to imaging SiR-DNA (Lukinavicius et al., 2015) (Spirochrome AG, Stein am Rhein, Switzerland) was added to a final concentration of 150 nM.

**Immunocytochemistry.** Cells were fixed with ice-cold methanol for 3 min, washed 3 times with phosphate buffer saline (PBS), followed by 15 min permeabilization with 0.5% Triton in PBS. Cells were washed 3 times with PBS and blocked in 1% Normal Goat Serum (NGS) exept in experiment for intensity of opto-PRC1 where cells were blocked in BSA in PBS for 1 h at 4°C. Cells were washed 3 times with PBS and then incubated in primary antibody solution in blocking buffer over night at 4°C. Following primary antibodies were used: mouse anti-PRC1 monoclonal antibody (1:100; C-1; sc-376983, Santa Cruz Biotechnology, Dallas, TX, USA), rabbit anti-α-tubulin polyclonal antibody (1:100; SAB4500087, Sigma-Aldrich Corporation, St. Louis, MO, USA), mouse monoclonal anti-Kif4A antibody (1:100; E-8; sc-365144, Santa Cruz Biotechnology, Dallas, TX, USA), rabbit polyclonal anti-MKLP1 antibody (1:100; N-19; sc-867, Santa Cruz Biotechnology, Dallas, TX, USA), mouse monoclonal anti-Eg5 antibody (1:100; A-1; sc-365681, Santa Cruz Biotechnology, Dallas, TX, USA). After washing of primary antibodies with PBS, cells were incubated in a solution of secondary antibodies in 2% NGS or BSA in PBS for 1 h at room temperature protected from light. Following secondary antibodies were used: donkey anti-mouse IgG Alexa Fluor 488 (1:250; ab150109, Abcam, Cambridge, UK), donkey anti-rabbit IgG Alexa Fluor 594 (1:250; ab150064, Abcam), donkey anti-rabbit IgG Alexa Fluor 405 (1:250; ab175649, Abcam), and goat anti-mouse IgG Alexa Fluor 647 (1:250; ab150119, Abcam). After washing of the secondary antibodies 3 times in PBS, cells were incubated with a solution of 4',6-diamidino-2-phenylindole (DAPI) (1:1000) in PBS for 20 min and washed 3 times in PBS or SiR-DNA (150 nM) in PBS for 15 min before imaging.

**Microscopy.** Immunocytochemistry imaging and live imaging of unlabeled U2OS, U2OS stably expressing CENPA-GFP, HeLa-TDS pEGFP-α-tubulin and HeLa BAC CENP-E-GFP cells was performed using Bruker Opterra Multipoint Scanning Confocal Microscope (Bruker Nano Surfaces, Middleton, WI, USA), described previously (Buda et al., 2017). In brief, the system was mounted on a Nikon Ti-E inverted microscope equipped with a Nikon CFI Plan Apo VC 100x/1.4 numerical aperture oil objective (Nikon, Tokyo, Japan). During imaging, live cells were maintained at 37°C using H301-K-frame heating chamber (Okolab, Pozzuoli,

NA, Italy). In order to obtain the optimal balance between spatial resolution and signal-to-noise ratio, 60-µm pinhole aperture was used. Opterra Dichroic and Barrier Filter Set 405/488/561/640 was used to separate the excitation light from the emitted fluorescence. Following emission filters were used: BL HC 525/30, BL HC 600/37 and BL HC 673/11 (all from Semrock, Rochester, NY, USA). Images were captured with an Evolve 512 Delta Electron Multiplying Charge Coupled Device (EMCCD) Camera (Photometrics, Tucson, AZ, USA) using a 200 ms exposure time. Electron multiplying gain was set on 400. Camera readout mode was 20 MHz. No binning was performed. The xy-pixel size in the image was 83 nm. The system was controlled with the Prairie View Imaging Software (Bruker).

For kinetics experiments on U2OS cells (**Fig. 1**), 561 and 488 nm diode laser lines were used every 10 s with 200 ms exposure time. In all other optogenetic experiments, stacks were acquired using sequentially the following diode laser lines: 561 nm (to visualize opto-PRC1), 488 nm (to activate the optogenetic system and to visualize GFP), and 640 nm (to visualize SiR-tubulin or SiR-DNA, when applicable), with time interval between z-stacks of 60 s and with 200 ms exposure time per laser line. To prevent dissociation of PRC1 from the cell membrane between acquiring two consecutive z-stacks, only blue light was turned on for 200 ms every 10 seconds. Cells were imaged this way for 20 min in order to achieve almost complete removal of PRC1 from the spindle, after which the blue light was turned off and imaging was continued for another 10 min at 60 s intervals. The total imaging time of 30 min was chosen to be close to the typical metaphase duration of 29.7 ± 2.3 min, which was measured from the metaphase plate formation until anaphase onset in U2OS cells expressing CENP-A-GFP, mCherry-α-tubulin and PA-GFP-tubulin (N=187) imaged after nuclear envelope breakdown every minute by obtaining 15 z-slices with 0.5 µm spacing and 150 ms exposure time. After 30 min of imaging, one z-stack in each of the three channels was taken in order to visualize the spindle and kinetochores after PRC1 return. In all cells except HeLa cells expressing pEGFP-α-tubulin, three focal planes with spacing between adjacent planes of 1 µm were acquired. Live imaging of HeLa cells stably expressing pEGFP-α-tubulin was performed in the same manner as described above for optogenetic experiments. Additionally, before turning the blue light on every 10 s, one z-stack was acquired using 561, 488 and 640 nm diode laser lines with averaging 8, and seven focal planes with spacing between adjacent planes of 0.5 µm. Stack was taken in the same way after 20 min of exposure to the blue light and again 10 min after the blue light was switched off. Imaging of HeLa BAC CENP-E-GFP mock and PRC1 siRNA treated cells was performed by acquiring one z-stack of 3 focal planes

with spacing between adjacent planes of 1 µm. For imaging of immunostained cells, 5 focal planes with spacing between adjacent planes of 0.5 µm were acquired.
Live imaging of unlabeled, BAC (except CENP-E-GFP), YFP-tubulin and EGFP-CLASP1 HeLa cell lines was performed on Leica TCS SP8 X laser scanning confocal microscope with a HC PL APO 63x/1.4 oil immersion objective (Leica, Wetzlar, Germany) heated with an objective integrated heater system (Okolab, Burlingame, CA, USA). During imaging, cells were maintained at 37°C in Okolab stage top heating chamber (Okolab, Burlingame, CA, USA). The system was controlled with the Leica Application Suite X software (LASX, 1.8.1.13759, Leica, Wetzlar, Germany). For GFP- and YFP-labeled proteins, a 488-nm and 514-nm Argon laser was used, respectively, and for SiR-DNA or SiR-tubulin, a 652-nm white light laser was used. GFP and SiR-DNA or SiR-tubulin emissions were detected with hybrid detector. For mock and PRC1 siRNA experiments, images were acquired at 2–3 focal planes with 1 µm spacing and 0.05-µm pixel size. In optogenetic experiments 3 z-stacks with 1 µm spacing were acquired sequentially every 10 s in the same manner as in optogenetic experiments in U2OS cells. One z-stack with line averaging of 6 or 16 was acquired before system activation, 20 min after exposure to blue light and 10 min after the light was switched off.
**Image and data analysis.** Since the cells were transiently transfected with opto-PRC1, we observed variability in PRC1 expression levels and therefore we imaged and analyzed only those metaphase spindles with PRC1 localization consistent with endogenous and fluorescently labeled PRC1 (Kajtez et al., 2016; Polak et al., 2017). Cells were not synchronized in order to avoid additional chemical treatment of cells, and metaphase was determined by alignment of kinetochores in the equatorial plane.

For determination of kinetics of PRC1 removal and return (**Fig. 1 C**), intensity of opto-PRC1 was measured in each time frame on one focal plane. We used *Poligon selection* tool in Fiji (National Institutes of Health, Bethesda, MD, USA) to encompass the area of the spindle, $A_{spindle}$, and measure mean spindle intensity, $M_{spindle}$. Mean background intensity in the cytoplasm was measured using 30 x 30 pixels rectangle, $M_{cyto}$. Spindle intensity was background corrected by subtracting $M_{cyto}$ from $M_{spindle}$ to obtain $M_{spindle\ corr}$. In order to calculate the sum of PRC1 intensity on the spindle, $M_{spindle\ corr}$ was multiplied with $A_{spindle}$ for each timeframe. The background intensity outside of the cell was negligible, thus we did not take it into account. Note that for the measurements of kinetic parameters in **Fig. 1 C**, four outliers were excluded (see **Fig. S1 E**). The percentage of PRC1 removal was calculated from the mean value of intensity of all cells at time 20 min, i.e., the last time point of the

continuous exposure to the blue light. The percentage of return was calculated from the mean value of intensity of all cells in the interval 25-30 min, i.e., during last 5 min of PRC1 return.

Intensity profiles of opto-PRC1 removal and return (**Fig. 1 D**) were obtained on sum intensity projections of all three z-planes by drawing a pole-to-pole line along the long axis of the spindle by using *Line* tool in Fiji. The width of the line corresponded to the width of each individual spindle. Intensities were normalized to position of the poles.

For quantification of PRC1 knock-down by siRNA and intensity level of opto-PRC1 (in **Fig. S1 A,B**) PRC1 intensity on fixed cells was measured on a sum-intensity projection of five focal planes by the procedure described above, in a way that mean spindle intensity was background corrected by subtracting mean intensity in the cytoplasm. For measuring opto-PRC1 intensity on the spindle cells where PRC1 was visible on astral microtubules were not analyzed, nor imaged in live experiments.

The GFP-tubulin signal intensity of a cross-section of a bridging fiber was measured by drawing a 3-pixel-thick line between and perpendicular to the tubulin signal joining the tips of sister k-fibers. The intensity profile was taken along this line and the mean value of the background signal present in the cytoplasm was subtracted from it. The signal intensity of the bridging fiber was calculated as the area under the peak using SciDavis (Free Software Foundation Inc., Boston, MA, USA). The signal intensity in the region lateral from k-fiber tip was measured in a similar manner, 1 µm away from a k-fiber tip, perpendicular to and crossing the corresponding k-fiber. All of the measurements were performed on a single z-plane. The profile intensity of bridging fiber and at the position lateral from k-fiber tip in SiR-tubulin (**Fig. 3 B,C**) was performed in the same manner. Note that mostly outermost fibers were used for these measurements because of being most easily distinguished from neighboring fibers.

Shapes of the spindle were quantified by tracking outermost k-fiber contours in the central z-slice of the spindle, or maximum intensity z-projection of two central z-slices. All spindles were rotated to have horizontal long axis. Pole-to-k-fiber-tip tracking was done using *Multipoint* tool by placing 5 roughly equidistant points along contour length, first point being at the pole and the last point being at the k-fiber tip. First point of each contour was translated to (0,0). This was done for maximum of 4 trackable outermost k-fibers in the spindle. Curvature of the contour was calculated by fitting a circle to the contour points of individual k-fibers and retrieving reciprocal value of its radius. To test the effect of tracking errors on curvature, we introduced 1-pixel noise to the x and y values of tracked points, which did not

change the result. Angle between outermost k-fibers (θ) was calculated as the angle between lines passing through last two points along the contour of sister k-fibers.

Spindle length and width were measured using *Line* tool in Fiji. For length measurements, a line was drawn from pole to pole. The position of the pole was defined as the location of the strongest tubulin signal. Width was measured by drawing a line between outermost kinetochore pairs on the opposite sides of the spindle, perpendicular to the spindle long axis.

The area of DNA was measured using *Poligon selection* tool in Fiji on sum-intensity projections of 3 and 7 z-planes for U2OS and HeLa GFP-α-tubulin cells, respectively, by encompassing chromosomes in SiR-DNA channel. The values were normalized to the value measured in 0 min for each cell.

Inter-kinetochore distance was measured using *Line* tool in Fiji on individual or maximum intensity z-projections of up to two z-planes as a distance between centers of sister kinetochore signals. Peripheral kinetochores were defined as three outermost pairs on each side of the spindle with respect to spindle long axis, while the remaining were considered as central. Measurement of inter-kinetochore distances in prometaphase was performed on U2OS cells expressing CENP-A-GFP, mCherry-α-tubulin and PA-GFP-tubulin, just after nuclear envelope breakdown in one imaging plane where both sister kinetochores could be clearly distinguished. For measuring kinetochore alignment and orientation, as well as orientation and length of PRC1 bundles, *Multipoint* tool in Fiji was used. A point was placed in the center of signal of each sister kinetochore or edges of PRC1 signal for each bundle. Before measuring, images were rotated in order to achieve perpendicular direction of the equatorial plane with respect to x-axis. The equatorial plane was defined with two points placed between outermost pairs of kinetochores on the opposite sides of the spindle. For all measurements regarding kinetochores, those located at the spindle poles were not taken into account. All measurements in opto and control cells were performed in three time-points: before the blue light was switched on, after 20 min of continuous exposure to the blue light, and 10 min after the blue light was turned off. In untreated and PRC1 siRNA treated cells measurements were performed at the beginning of imaging.

The intensity of GFP-Kif4A in metaphase and anaphase was measured in GFP-Kif4A channel on sum-intensity projections of all three z-planes using *Poligon selection* tool in Fiji by encompassing chromosomes in SiR-DNA channel. The intensity of opto-PRC1 in metaphase was measured by encompassing the spindle area. Background cytoplasm intensities in both GFP-Kif4A and opto-PRC1 channels were measured in 30 x 30 pixels

rectangle and subtracted from measured mean intensities of GFP-Kif4A and opto-PRC1. Corrected intensities were divided by the number of focal planes. Measurements were performed in three time-points in metaphase: before the blue light was switched on, after 20 min of continuous exposure to the blue light, and 10 min after the blue light was turned off. In anaphase, measurements were performed 4 min after anaphase onset. Anaphase onset was defined as the timeframe when separation of majority of sister chromatids in SiR-DNA channel occurred.

The mean signal intensities of opto-PRC1 and MKLP1-GFP were measured on the central z-plane using *Poligon selection* tool in Fiji by encompassing the spindle area in SiR-tubulin channel. Background cytoplasm intensities in both channels were measured in 30 x 30 pixels rectangle and subtracted from measured mean intensities of opto-PRC1and MKLP1-GFP. Measurements were performed in the same time-points as for Kif4A in metaphase.

For quantification of PRC1 knock-down by siRNA in HeLa BAC MKLP1-GFP cell line, PRC1 intensity was quantified in the same manner as in U2OS cells. The intensity levels of MKLP1-GFP and Kif4A-GFP in fixed HeLa cells were measured by encompassing the whole cell area using *Poligon selection* tool in Fiji on sum intensity projections of 5 z-planes.

Statistical analysis was performed in MATLAB (MathWorks, Natick, MA, USA) and RStudio (R Foundation for Statistical Computing, Vienna, Austria). Normality of the data was inspected by Q-Q plots and Shapiro-Wilk test of normality. Normally distributed data were tested with two-tailed t-test, while Mann-Whitney test was used for non-normally distributed data, as noted in figure captions. Proportions were statistically compared with test for equality of proportions, two-proportions z-test. For data with expected count smaller than 5, Yates's correction for continuity was used.

Graphs were generated in MATLAB (MathWorks) and RStudio (R Foundation for Statistical Computing). ImageJ (National Institutes of Health, Bethesda, MD, USA) was used to crop and rotate images, and to adjust brightness and contrast to the entire image, which was applied equally to all images in the same panel. Figures were assembled in Adobe Illustrator CS5 (Adobe Systems, Mountain View, CA, USA).

**Acknowledgements**

We thank Helder Maiato and Marin Barišić for U2OS cell line; Ina Poser and Tony Hyman for HeLa MKLP1-GFP, Kif4A-GFP, Kif18A-GFP, and CENP-E-GFP cell lines; Helder Maiato for HeLa EGFP-CLASP1 cell line; Lars Jansen for HeLa YFP-tubulin cell line; Marin Barišić for GFP- CENP-E plasmid; Jason Stumpff for pEGFP-C1Kif4a-sires and EGFP-

Kif18A plasmids; the entire Tolić and Pavin group for discussions and constructive comments on the manuscript; Sonja Lesjak for help with the cloning and plasmids; Ivana Šarić for the drawings. This work was funded by European Research Council (ERC, GA number 647077) and Croatian Science Foundation (HRZZ, project IP-2014-09-4753).

**Author Contributions**

M.J, P.R. and J.M. performed and analyzed all experiments, and wrote the manuscript together with I.M.T. A.M. made the optogenetic plasmid and performed pilot experiments. I.M.T. conceived and supervised the project.

**Competing Interests Statement**

The authors declare no competing interests.

**Data availability.**

All data are available from the corresponding author upon request.

**Code availability.**

Custom codes used in this study are available upon request.

**References**

Al-Bassam, J., H. Kim, G. Brouhard, A. van Oijen, S.C. Harrison, and F. Chang. 2010. CLASP promotes microtubule rescue by recruiting tubulin dimers to the microtubule. *Dev. Cell*. 19:245-258.

Armond, J.W., E.F. Harry, A.D. McAinsh, and N.J. Burroughs. 2015. Inferring the Forces Controlling Metaphase Kinetochore Oscillations by Reverse Engineering System Dynamics. *PLoS Comput. Biol.* 11:e1004607.

Barisic, M., P. Aguiar, S. Geley, and H. Maiato. 2014. Kinetochore motors drive congression of peripheral polar chromosomes by overcoming random arm-ejection forces. *Nat. Cell Biol.* 16:1249-1256.

Bieling, P., I.A. Telley, and T. Surrey. 2010. A minimal midzone protein module controls formation and length of antiparallel microtubule overlaps. *Cell*. 142:420-432.

Buda, R., K. Vukusic, and I.M. Tolic. 2017. Dissection and characterization of microtubule bundles in the mitotic spindle using femtosecond laser ablation. *Methods Cell Biol.* 139:81-101.

Cai, S., C.B. O'Connell, A. Khodjakov, and C.E. Walczak. 2009. Chromosome congression in the absence of kinetochore fibres. *Nat. Cell Biol.* 11:832-838.

Cheeseman, L.P., E.F. Harry, A.D. McAinsh, I.A. Prior, and S.J. Royle. 2013. Specific removal of TACC3-ch-TOG-clathrin at metaphase deregulates kinetochore fiber tension. *J. Cell Sci.* 126:2102-2113.
David, A.F., P. Roudot, W.R. Legant, E. Betzig, G. Danuser, and D.W. Gerlich. 2019. Augmin accumulation on long-lived microtubules drives amplification and kinetochore-directed growth. *J. Cell Biol*. 218:2150-2168.
Elting, M.W., M. Prakash, D.B. Udy, and S. Dumont. 2017. Mapping Load-Bearing in the Mammalian Spindle Reveals Local Kinetochore Fiber Anchorage that Provides Mechanical Isolation and Redundancy. *Curr. Biol.* 27:2112-2122.
Fielmich, L.E., R. Schmidt, D.J. Dickinson, B. Goldstein, A. Akhmanova, and S. van den Heuvel. 2018. Optogenetic dissection of mitotic spindle positioning in vivo. *Elife*. 7:e38198.
Gruneberg, U., R. Neef, X. Li, E.H. Chan, R.B. Chalamalasetty, E.A. Nigg, and F.A. Barr. 2006. KIF14 and citron kinase act together to promote efficient cytokinesis. *J. Cell Biol.* 172:363-372.
Gudimchuk, N., B. Vitre, Y. Kim, A. Kiyatkin, D.W. Cleveland, F.I. Ataullakhanov, and E.L. Grishchuk. 2013. Kinetochore kinesin CENP-E is a processive bi-directional tracker of dynamic microtubule tips. *Nat. Cell Biol*. 15:1079-1088.
Guntas, G., R.A. Hallett, S.P. Zimmerman, T. Williams, H. Yumerefendi, J.E. Bear, and B. Kuhlman. 2015. Engineering an improved light-induced dimer (iLID) for controlling the localization and activity of signaling proteins. *Proc. Natl. Acad. Sci. USA*. 112:112-117.
Haruki, H., J. Nishikawa, and U.K. Laemmli. 2008. The anchor-away technique: rapid, conditional establishment of yeast mutant phenotypes. *Mol. Cell*. 31:925-932.
Janson, M.E., R. Loughlin, I. Loiodice, C. Fu, D. Brunner, F.J. Nedelec, and P.T. Tran. 2007. Crosslinkers and motors organize dynamic microtubules to form stable bipolar arrays in fission yeast. *Cell*. 128:357-368.
Jiang, W., G. Jimenez, N.J. Wells, T.J. Hope, G.M. Wahl, T. Hunter, and R. Fukunaga. 1998. PRC1: a human mitotic spindle-associated CDK substrate protein required for cytokinesis. *Mol. Cell*. 2:877-885.
Kajtez, J., A. Solomatina, M. Novak, B. Polak, K. Vukusic, J. Rudiger, G. Cojoc, A. Milas, I. Sumanovac Sestak, P. Risteski, F. Tavano, A.H. Klemm, E. Roscioli, J. Welburn, D. Cimini, M. Gluncic, N. Pavin, and I.M. Tolic. 2016. Overlap microtubules link sister k-fibres and balance the forces on bi-oriented kinetochores. *Nat. Commun.* 7:10298.
Kapoor, T.M., M.A. Lampson, P. Hergert, L. Cameron, D. Cimini, E.D. Salmon, B.F. McEwen, and A. Khodjakov. 2006. Chromosomes can congress to the metaphase plate before biorientation. *Science*. 311:388-391.
Kellogg, E.H., S. Howes, S.C. Ti, E. Ramirez-Aportela, T.M. Kapoor, P. Chacon, and E. Nogales. 2016. Near-atomic cryo-EM structure of PRC1 bound to the microtubule. *Proc. Natl. Acad. Sci. USA*. 113:9430-9439.
Kurasawa, Y., W.C. Earnshaw, Y. Mochizuki, N. Dohmae, and K. Todokoro. 2004. Essential roles of KIF4 and its binding partner PRC1 in organized central spindle midzone formation. *EMBO J.* 23:3237-3248.
Liu, J., Z. Wang, K. Jiang, L. Zhang, L. Zhao, S. Hua, F. Yan, Y. Yang, D. Wang, C. Fu, X. Ding, Z. Guo, and X. Yao. 2009. PRC1 cooperates with CLASP1 to organize central spindle plasticity in mitosis. *J. Biol. Chem.* 284:23059-23071.
Lukinavicius, G., C. Blaukopf, E. Pershagen, A. Schena, L. Reymond, E. Derivery, M. Gonzalez-Gaitan, E. D'Este, S.W. Hell, D. Wolfram Gerlich, and K. Johnsson. 2015. SiR-Hoechst is a far-red DNA stain for live-cell nanoscopy. *Nat. Commun.* 6:8497.
Lukinavicius, G., L. Reymond, E. D'Este, A. Masharina, F. Gottfert, H. Ta, A. Guther, M. Fournier, S. Rizzo, H. Waldmann, C. Blaukopf, C. Sommer, D.W. Gerlich, H.D. Arndt, S.W.

Hell, and K. Johnsson. 2014. Fluorogenic probes for live-cell imaging of the cytoskeleton. *Nat. Methods*. 11:731-733.
Maiato, H., E.A. Fairley, C.L. Rieder, J.R. Swedlow, C.E. Sunkel, and W.C. Earnshaw. 2003. Human CLASP1 is an outer kinetochore component that regulates spindle microtubule dynamics. *Cell*. 113:891-904.
Maiato, H., A.M. Gomes, F. Sousa, and M. Barisic. 2017. Mechanisms of Chromosome Congression during Mitosis. *Biology (Basel)*. 6:13.
Mann, B.J., and P. Wadsworth. 2018. Distribution of Eg5 and TPX2 in mitosis: Insight from CRISPR tagged cells. *Cytoskeleton (Hoboken)*. 75:508-521.
Mastronarde, D.N., K.L. McDonald, R. Ding, and J.R. McIntosh. 1993. Interpolar spindle microtubules in PTK cells. *J. Cell Biol.* 123:1475-1489.
Mayr, M.I., S. Hummer, J. Bormann, T. Gruner, S. Adio, G. Woehlke, and T.U. Mayer. 2007. The human kinesin Kif18A is a motile microtubule depolymerase essential for chromosome congression. *Curr. Biol*. 17:488-498.
McEwen, B.F., G.K. Chan, B. Zubrowski, M.S. Savoian, M.T. Sauer, and T.J. Yen. 2001. CENP-E is essential for reliable bioriented spindle attachment, but chromosome alignment can be achieved via redundant mechanisms in mammalian cells. *Mol. Biol. Cell*. 12:2776-2789.
Milas, A., M. Jagric, J. Martincic, and I.M. Tolic. 2018. Optogenetic reversible knocksideways, laser ablation, and photoactivation on the mitotic spindle in human cells. *Methods Cell Biol.* 145:191-215.
Milas, A., and I.M. Tolic. 2016. Relaxation of interkinetochore tension after severing of a k-fiber depends on the length of the k-fiber stub. *Matters Select*:201603000025.
Mollinari, C., J.P. Kleman, W. Jiang, G. Schoehn, T. Hunter, and R.L. Margolis. 2002. PRC1 is a microtubule binding and bundling protein essential to maintain the mitotic spindle midzone. *J. Cell Biol.* 157:1175-1186.
Mollinari, C., J.P. Kleman, Y. Saoudi, S.A. Jablonski, J. Perard, T.J. Yen, and R.L. Margolis. 2005. Ablation of PRC1 by small interfering RNA demonstrates that cytokinetic abscission requires a central spindle bundle in mammalian cells, whereas completion of furrowing does not. *Mol. Biol. Cell*. 16:1043-1055.
Neef, R., U. Gruneberg, R. Kopajtich, X. Li, E.A. Nigg, H. Sillje, and F.A. Barr. 2007. Choice of Plk1 docking partners during mitosis and cytokinesis is controlled by the activation state of Cdk1. *Nat. Cell Biol.* 9:436-444.
Nixon, F.M., C. Gutierrez-Caballero, F.E. Hood, D.G. Booth, I.A. Prior, and S.J. Royle. 2015. The mesh is a network of microtubule connectors that stabilizes individual kinetochore fibers of the mitotic spindle. *Elife*. 4:e07635.
O'Neill, P.R., V. Kalyanaraman, and N. Gautam. 2016. Subcellular optogenetic activation of Cdc42 controls local and distal signaling to drive immune cell migration. *Mol. Biol. Cell*. 27:1442-1450.
O'Toole, E., M. Morphew, and J.R. McIntosh. 2019. Electron tomography reveals aspects of spindle structure important for mechanical stability at metaphase. *Mol. Biol. Cell.* 31:mbcE19070405.
Okumura, M., T. Natsume, M.T. Kanemaki, and T. Kiyomitsu. 2018. Dynein-Dynactin-NuMA clusters generate cortical spindle-pulling forces as a multi-arm ensemble. *Elife*. 7:e36559.
Polak, B., P. Risteski, S. Lesjak, and I.M. Tolic. 2017. PRC1-labeled microtubule bundles and kinetochore pairs show one-to-one association in metaphase. *EMBO Rep.* 18:217-230.
Rieder, C.L., E.A. Davison, L.C. Jensen, L. Cassimeris, and E.D. Salmon. 1986. Oscillatory movements of monooriented chromosomes and their position relative to the spindle pole result from the ejection properties of the aster and half-spindle. *J. Cell Biol*. 103:581-591.

Rieder, C.L., and E.D. Salmon. 1994. Motile kinetochores and polar ejection forces dictate chromosome position on the vertebrate mitotic spindle. *J. Cell Biol*. 124:223-233.
Robinson, M.S., D.A. Sahlender, and S.D. Foster. 2010. Rapid inactivation of proteins by rapamycin-induced rerouting to mitochondria. *Dev. Cell*. 18:324-331.
Schaar, B.T., G.K. Chan, P. Maddox, E.D. Salmon, and T.J. Yen. 1997. CENP-E function at kinetochores is essential for chromosome alignment. *J. Cell Biol*. 139:1373-1382.
Stumpff, J., G. von Dassow, M. Wagenbach, C. Asbury, and L. Wordeman. 2008. The kinesin-8 motor Kif18A suppresses kinetochore movements to control mitotic chromosome alignment. *Dev. Cell*. 14:252-262.
Stumpff, J., M. Wagenbach, A. Franck, C.L. Asbury, and L. Wordeman. 2012. Kif18A and chromokinesins confine centromere movements via microtubule growth suppression and spatial control of kinetochore tension. *Dev. Cell*. 22:1017-1029.
Subramanian, R., S.C. Ti, L. Tan, S.A. Darst, and T.M. Kapoor. 2013. Marking and measuring single microtubules by PRC1 and kinesin-4. *Cell*. 154:377-390.
Subramanian, R., E.M. Wilson-Kubalek, C.P. Arthur, M.J. Bick, E.A. Campbell, S.A. Darst, R.A. Milligan, and T.M. Kapoor. 2010. Insights into antiparallel microtubule crosslinking by PRC1, a conserved nonmotor microtubule binding protein. *Cell*. 142:433-443.
Tolic, I.M. 2018. Mitotic spindle: kinetochore fibers hold on tight to interpolar bundles. *Eur. Biophys. J.* 47:191-203.
Tolic, I.M., and N. Pavin. 2016. Bridging the gap between sister kinetochores. *Cell Cycle*. 15:1169-1170.
van Haren, J., R.A. Charafeddine, A. Ettinger, H. Wang, K.M. Hahn, and T. Wittmann. 2018. Local control of intracellular microtubule dynamics by EB1 photodissociation. *Nat. Cell Biol.* 20:252-261.
Vukusic, K., R. Buda, A. Bosilj, A. Milas, N. Pavin, and I.M. Tolic. 2017. Microtubule Sliding within the Bridging Fiber Pushes Kinetochore Fibers Apart to Segregate Chromosomes. *Dev. Cell*. 43:11-23.
Wandke, C., M. Barisic, R. Sigl, V. Rauch, F. Wolf, A.C. Amaro, C.H. Tan, A.J. Pereira, U. Kutay, H. Maiato, P. Meraldi, and S. Geley. 2012. Human chromokinesins promote chromosome congression and spindle microtubule dynamics during mitosis. *J. Cell Biol.* 198:847-863.
Wang, H., and K.M. Hahn. 2016. LOVTRAP: A Versatile Method to Control Protein Function with Light. *Curr. Protoc. Cell Biol.* 73:21 10 21-21 10 14.
Waters, J.C., R.V. Skibbens, and E.D. Salmon. 1996. Oscillating mitotic newt lung cell kinetochores are, on average, under tension and rarely push. *J. Cell Sci.* 109:2823-2831.
Wendell, K.L., L. Wilson, and M.A. Jordan. 1993. Mitotic block in HeLa cells by vinblastine: ultrastructural changes in kinetochore-microtubule attachment and in centrosomes. *J. Cell Sci.* 104:261-274.
Wordeman, L., J. Decarreau, J.J. Vicente, and M. Wagenbach. 2016. Divergent microtubule assembly rates after short- versus long-term loss of end-modulating kinesins. *Mol. Biol. Cell*. 27:1300-1309.
Yang, X., A.P. Jost, O.D. Weiner, and C. Tang. 2013. A light-inducible organelle-targeting system for dynamically activating and inactivating signaling in budding yeast. *Mol. Biol. Cell*. 24:2419-2430.
Yu, N., L. Signorile, S. Basu, S. Ottema, J.H.G. Lebbink, K. Leslie, I. Smal, D. Dekkers, J. Demmers, and N. Galjart. 2016. Isolation of Functional Tubulin Dimers and of Tubulin-Associated Proteins from Mammalian Cells. *Curr. Biol*. 26:1728-1736.
Zhang, H., C. Aonbangkhen, E.V. Tarasovetc, E.R. Ballister, D.M. Chenoweth, and M.A. Lampson. 2017. Optogenetic control of kinetochore function. *Nat. Chem. Biol.* 13:1096-1101.

Zhu, C., and W. Jiang. 2005. Cell cycle-dependent translocation of PRC1 on the spindle by Kif4 is essential for midzone formation and cytokinesis. *Proc. Natl. Acad. Sci. USA*. 102:343-348.
Zhu, C., E. Lau, R. Schwarzenbacher, E. Bossy-Wetzel, and W. Jiang. 2006. Spatiotemporal control of spindle midzone formation by PRC1 in human cells. *Proc. Natl. Acad. Sci. USA*. 103:6196-6201.

## Supplementary Figures

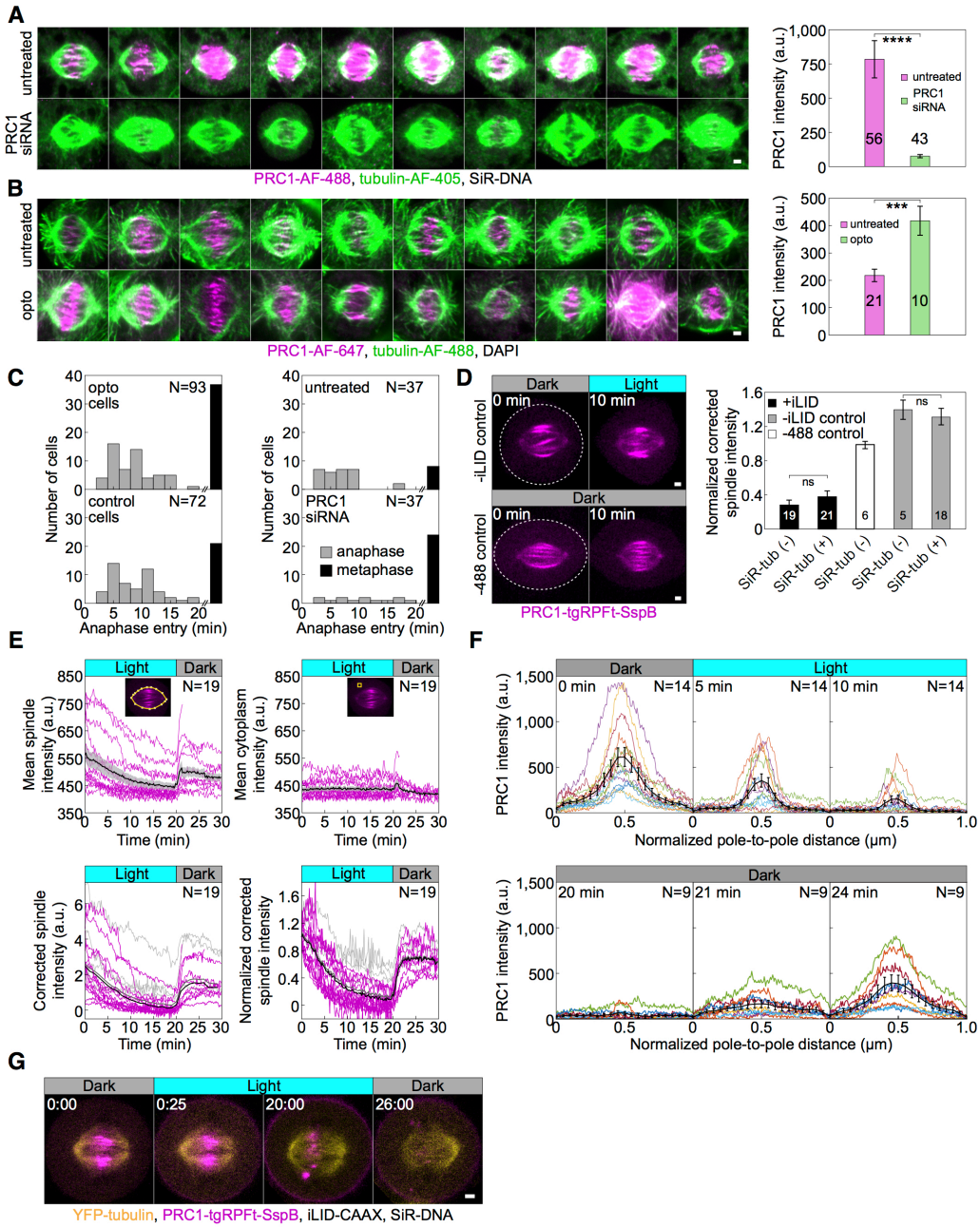


**Figure S1.**

(**A**) Metaphase spindles in fixed, unlabeled U2OS cells (left) immunostained for endogenous PRC1 (AF-488, magenta), tubulin (AF-405, green) and stained with SiR-DNA (not shown) in untreated (top) and PRC1 siRNA treated cells (bottom). All images are sum intensity projections of five z-planes. Graph (right) shows PRC1 intensity in untreated (magenta) and PRC1 (green) siRNA treated cells. Data obtained from three independent experiments. (**B**) Metaphase spindles in fixed, unlabeled U2OS cells immunostained for PRC1 (AF-647, magenta), tubulin (AF-488, green) and stained with DAPI (not shown) in untreated (top) and

PRC1 siRNA treated cells with addition of opto-PRC1 (bottom). All images are sum intensity projections of five z-planes. Graph (right) shows PRC1 intensity in untreated (magenta) and cells with depleted endogenous and added opto-PRC1 (green). Data obtained from two independent experiments. (**C**) Number of cells that entered anaphase (gray bars) and those remained in metaphase (black bars) during 20 min of exposure to the blue light for opto and control cells (left), and untreated and PRC1 siRNA treated cells (right). For opto and control cells those imaged for measurements of SiR-DNA area are also taken into account. (**D**) Time-lapse images of U2OS cells with stable expression of CENP-A-GFP (not shown) and transient expression of opto-PRC1 and iLID-CAAX, non-exposed to the blue light (-488 control, bottom left) and exposed to blue light but without iLID-CAAX (-iLID control, top left), before and after 10 minutes of imaging. Graph (right) shows opto-PRC1 intensities after 10 min of imaging in +iLID cells with and without SiR-tubulin (black), -488 control cells (white) and –iLID control cells with and without SiR-tubulin (gray). Note that SiR-tubulin does not affect opto-PRC1 removal. (**E**) Raw opto-PRC1 intensities from individual cells (magenta lines) at the metaphase spindle (top left) and in cytoplasm (top right) during removal and return to the spindle. Mean (thick black line) and s.e.m. (shaded area). Opto-PRC1 intensities at the metaphase spindle corrected for cytoplasm (bottom left) and normalized to the initial value (bottom right). Outliers (gray lines), mean without outliers (thick black line), mean with outliers (thick gray line). Note that outliers are excluded in **Fig. 1 C**. (**F**) Pole-to-pole opto-PRC1 intensity during removal (top) and return (bottom) to the spindle as in **Fig. 1 D**. Individual cells (colored lines), mean (thick black line), s.e.m (error bars). (**G**) Time-lapse image of a HeLa cell stably expressing YFP-tubulin (yellow), transiently opto-PRC1 (magenta) and iLID-CAAX, and stained with SiR-DNA dye (not shown). In 0:00 (Dark), 561 (opto-PRC1), and 514 (tubulin) + 652 (SiR-DNA) nm lasers are used stack-sequentially. From 0:25-20:00 (Light), 561 and 488+514+652 nm lasers are used stack-sequentially, every 25 s. Note that in 0:00 min, opto-PRC1 is not present on the membrane as in **Fig. 1 B**. However, in the first frame of Light sequence, 0:25, weak signal of opto-PRC1 is present on the membrane even though opto-PRC1 was imaged in stack before 488 nm laser was on. Also, opto-PRC1 is visible on the membrane 6 min after (26:00, Dark) 488 nm laser was turned off. This is a consequence of 514 nm laser, used to visualize YFP, being able to activate optogenetic system. Images are max projection of 3 z-planes.
N and numbers inside bars; number of cells. Scale bars; 2 µm. Statistical analysis; t-test. p-value legend as in **Fig. 2**.

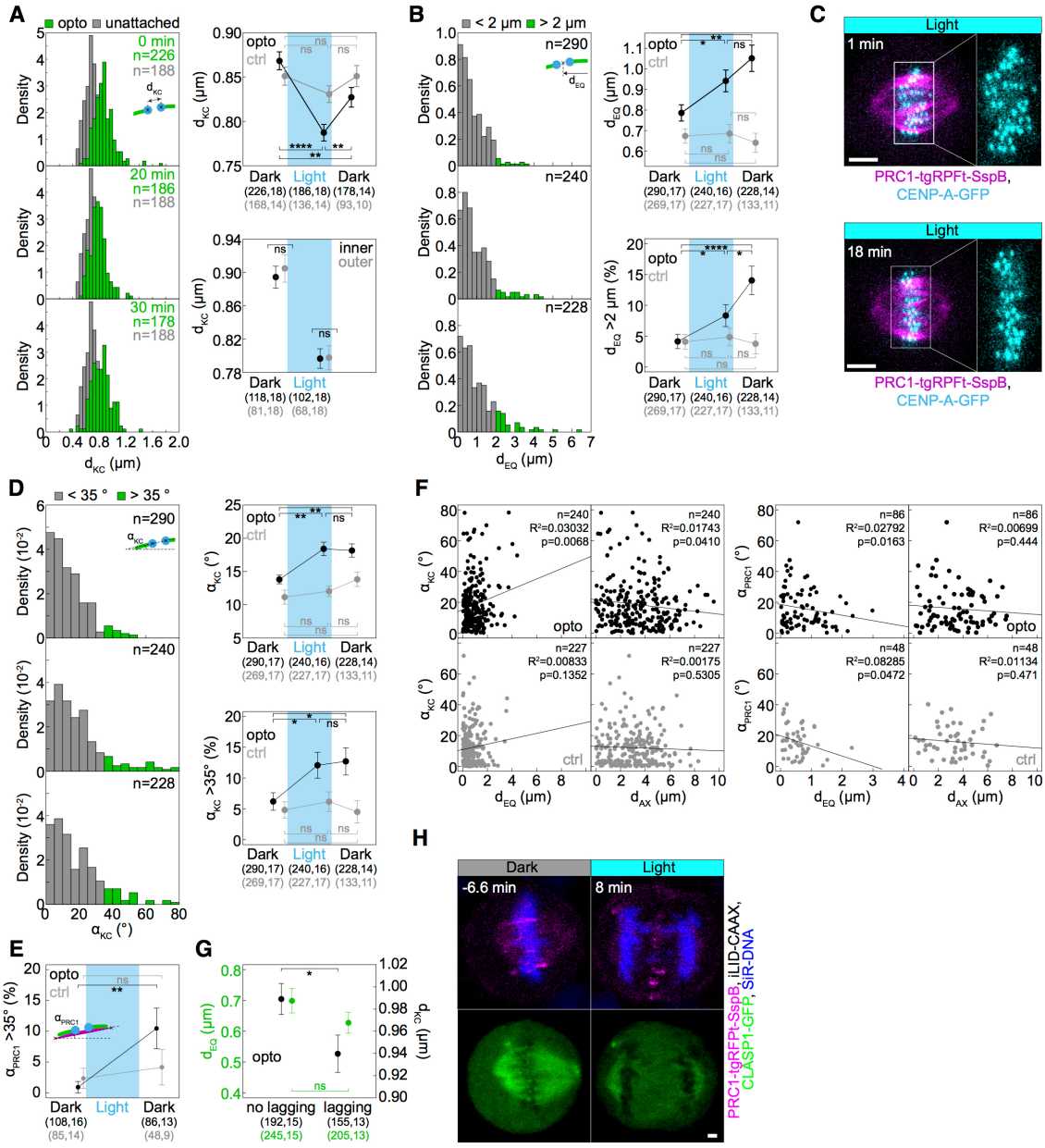


**Figure S2.**

(**A**) Density histograms (left) of $d_{KC}$ for opto U2OS cells (green), before (0 min, top), at the end of continuous exposure (20 min, middle) and 10 min after cessation of exposure to the blue light (30 min, bottom), overlaid on density histogram of unattached $d_{KC}$ from early prometaphase cells (mean: 0.66 ± 0.01 µm, N=7, n=188) (gray). Inter-kinetochore distance ($d_{KC}$) (top right) in control (gray) and opto cells with and without SiR-tubulin (black) in same timepoints. Inter-kinetochore distance ($d_{KC}$) (bottom right) of inner (black) and outer (gray) kinetochore pairs before and 20 min after exposure to the blue light. (**B**) Density histograms (left) of $d_{EQ}$ for opto U2OS cells for time-points as in **A**. $d_{EQ}$ greater (green) and lesser than 2

μm (gray) is shown. This corresponds to roughly 95$^{th}$ percentile of opto data before system activation. Percentage of $d_{EQ}$ greater than 2 μm in opto (black) and control (gray) cells (bottom right). Graph (top right) showing $d_{EQ}$ in control (gray) and opto cells with and without SiR-tubulin (black) in timepoints as in **A**. (**C**) Spindle in a U2OS cell stably expressing CENP-A-GFP (cyan) with transient expression of opto-PRC1 (magenta) at the beginning (1 min, top) and at the end of continuous exposure to the blue light (18 min, bottom). Enlargements of the boxed regions show kinetochores only. Images are maximum intensity projections of three z-planes, smoothed with 0.5-pixel Gaussian blur. (**D**) Density histogram (left) of $\alpha_{KC}$ for opto U2OS cells for time-points as in **A**. $\alpha_{KC}$ greater (green) and lesser than 35° (gray) is shown. This corresponds to roughly 95$^{th}$ percentile of opto data before system activation. Percentage of $\alpha_{KC}$ greater than 35° in opto (black) and control (gray) cells (bottom right). Graph (top right) showing $\alpha_{KC}$ in control (gray) and opto cells with and without SiR-tubulin (black) in timepoints as in **A**. (**E**) Percentage of $\alpha_{PRC1}$ greater than 35° in opto (black) and control (gray) cells before exposure and 10 min after cessation of exposure to the blue light. (**F**) Graphs show $\alpha_{KC}$ versus corresponding $d_{EQ}$ and $d_{AX}$ (left), and $\alpha_{PRC1}$ versus $d_{EQ}$ and $d_{AX}$ (right) in opto (top, black) and control (bottom, gray) cells. Kinetochore parameters correspond to 20 min after continuous exposure to the blue light, and PRC1 parameters correspond to 10 min after cessation of exposure. Note that PRC1 is not on the spindle at 20 min in opto cells. Black lines show linear regression. (**G**) $d_{KC}$ (black) and $d_{EQ}$ (green) in opto anaphase cells with and without lagging kinetochores. (**H**) Time-lapse images of HeLa cell stably expressing EGFP-CLASP1 with transient expression of opto-PRC1 (magenta) and iLID-CAAX, and stained with SiR-DNA (blue). Top (merge tgRFPt and SiR-DNA), bottom (GFP). Images are maximum intensity projections of 3 z-planes, smoothed with 0.5-pixel Gaussian blur. Anaphase onset is set as time 0 min. Note the absence of GFP signal in the spindle midzone and lagging chromosomes at 8 min.

Cyan rectangles inside graphs indicate exposure to the blue light. Numbers in brackets; number of measurements and cells, respectively. Time; min. n; number of measurements. Scale bars; 2 μm. Statistical analysis; two-proportions z-test. $R^2$, coefficient of determination. p-value legend as in **Fig. 2**.

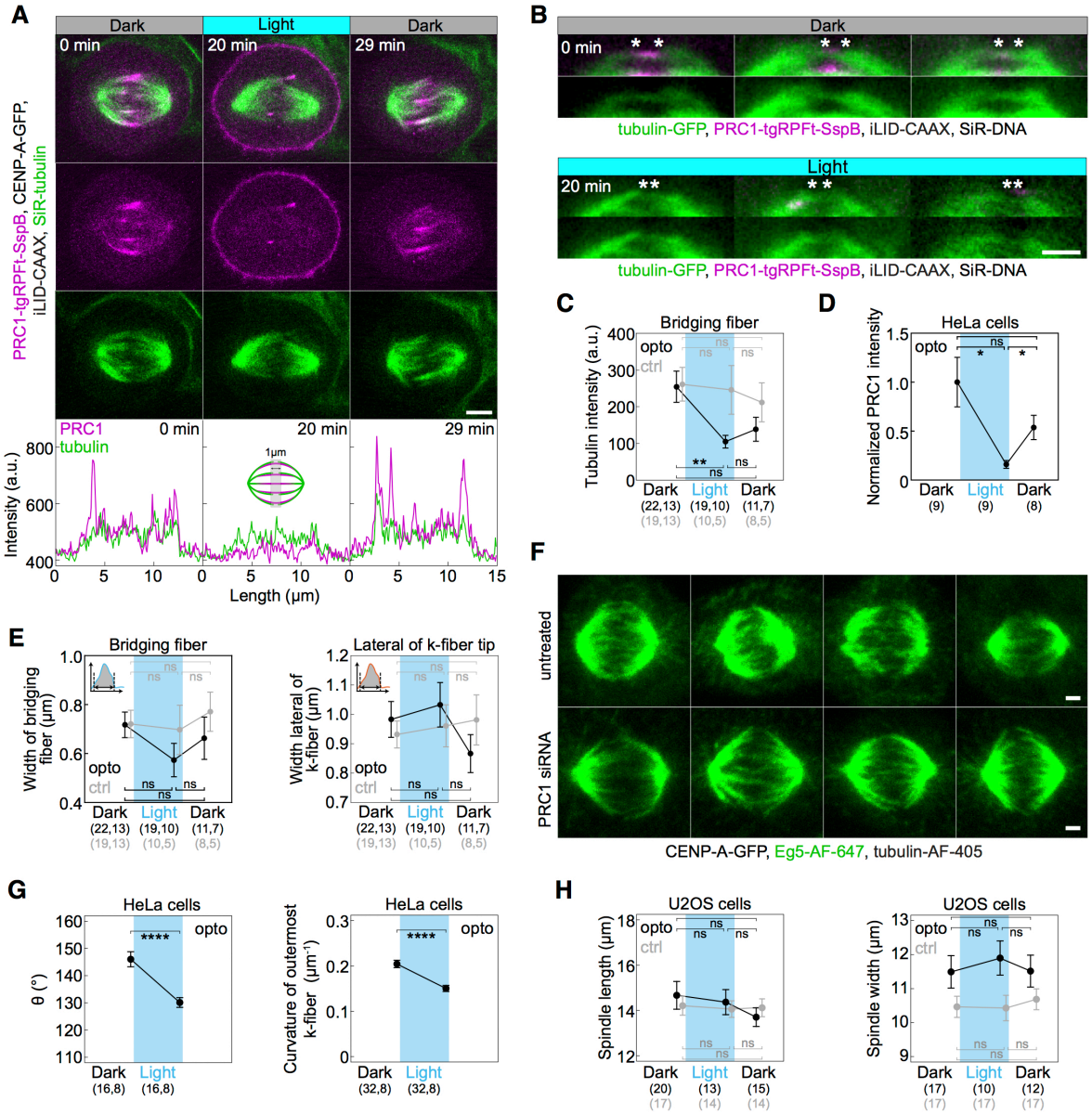


**Figure S3.**

(**A**) Spindle in a U2OS cell stably expressing CENP-A-GFP (not shown), with transient expression of opto-PRC1 (magenta) and iLID-CAAX, and stained with SiR-tubulin (green) before (0 min, Dark), at the end of continuous exposure (20 min, Light) and 9 min after cessation of exposure to the blue light (29 min, Dark). Top (merge), middle (tgRFPt), bottom (SiR). Graphs (bottom) correspond to signal intensity profiles of opto-PRC1 (magenta) and SiR-tubulin (green) taken across equatorial plane in shown spindles. Profile intensities were acquired on individual z-planes using a 1-µm thick line across the spindle midzone. Images are individual z-plane, smoothed with 0.5-pixel-radius Gaussian blur. Scale bar; 5 µm.

(**B**) Enlargements of spindles in HeLa cells with stable expression of tubulin-GFP (green), depleted for endogenous PRC1, with transient expression of opto-PRC1 (magenta) and iLID-

CAAX, and stained with SiR-DNA (not shown), before exposure to the blue light (0 min, Dark, top; first row: merge, second row: GFP) and at the end of continuous exposure to the blue light (20 min, Light, bottom; first row: merge, second row: GFP). Note that at 20 min opto-PRC1 is absent from the spindle. Images do not belong to the same cell. Asterisks mark the position of kinetochores. All images are single z-plane smoothed with 0.5-pixel-Gaussian blur. Scale bar; 2 µm.

(**C**) Tubulin-GFP signal intensity of the bridging fibers in opto (black) and control (gray) HeLa cells before (0 min, Dark), at the end of continuous exposure (20 min, Light) and 10 min after cessation of exposure to the blue light (30 min, Dark). Signal intensity is measured as the area under the peak shown in **Fig. 3 E**. (**D**) Graph showing normalized PRC1 intensity on the spindle in opto HeLa tubulin-GFP cells used for measurements in **C**. (**E**) Width of the bridging fiber (left) and microtubule bundle lateral from k-fiber tip (right) in opto (black) and control (gray) HeLa cells at time-points as in **C**, measured as shown in schemes (upper left corners). (**F**) Metaphase spindles in fixed U2OS cells stably expressing CENP-A-GFP (not shown) immunostained for Eg5 (AF-647, green) and tubulin (AF-405, not shown) in untreated (top) and PRC1 siRNA treated cells (bottom). All images are sum intensity projections of five z-planes. Scale bar; 2 µm. (**G**) Angle between (left) and curvature (right) of the outermost k-fibers in HeLa cells. Measured as in scheme in **Fig. 3 I**. (**H**) Spindle length (left) and width (right) in opto (black) and control (gray) U2OS cells at timepoints as in **C**. Cyan rectangles inside graphs indicate exposure to the blue light. Numbers in brackets; number of measurements and cells, respectively. Statistical analysis; t-test. p-value legend as in **Fig. 2**.

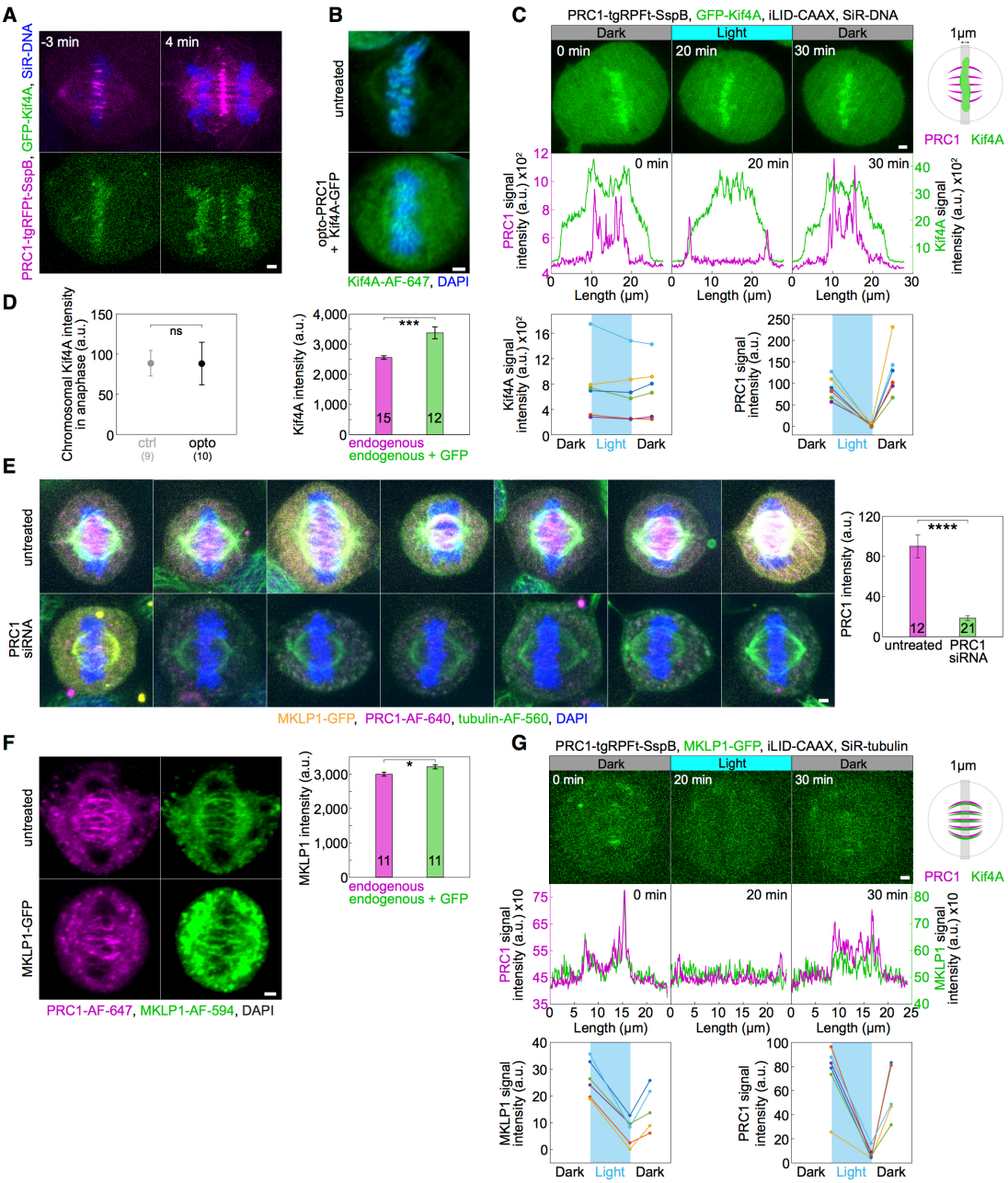


**Figure S4.**

(**A**) Time-lapse images of U2OS cells with transient expression of opto-PRC1 (magenta) and GFP-Kif4A (green). Top (merge tgRFPt and SiR-DNA), bottom (GFP). Anaphase onset is set as time 0 min. (**B**) Spindle in a fixed untreated unlabeled U2OS cell (top) and unlabeled U2OS cell, depleted for endogenous PRC1 and transiently expressing Kif4A-GFP (not shown) and opto-PRC1 (not shown) (middle), immunostained for Kif4A (AF-647, green) and stained with DAPI (blue). Images are sum-intensity projections of 5 z-planes smoothed with 0.5-pixel-Gaussian blur. Graph (bottom) shows Kif4A intensity in untreated (magenta) and cells with transient expression of Kif4A-GFP (green). The signal intensity of Kif4A in these

cells was 30% higher compared to endogenous Kif4A. (**C**) Time-lapse of U2OS cell as in **Fig. 4 A** (only GFP-Kif4A channel) (top). Graphs (middle) correspond to membrane-to-membrane intensity profiles of GFP-Kif4A (green) and opto-PRC1 (magenta) retrieved from the same position perpendicular to the midzone and in time-points as in **Fig. 4 A**, acquired by 1-µm wide line on a single z-plane. Schematic representation of performed measurement is given on the right. Graphs (bottom) show individual GFP-Kif4A (left) and opto-PRC1 (right) intensities. (**D**) GFP-Kif4A intensity on chromosomes in opto (black) and control (gray) cells 4 min after anaphase onset. Anaphase onset is defined as a timeframe of sister chromatid separation. Numbers in brackets; number of cells. (**E**) Spindles in fixed HeLa cells stably expressing MKLP1-GFP (yellow) and immunostained for PRC1 (AF-640, magenta), tubulin (AF-560, green) and stained with DAPI (blue) in untreated (top) and PRC1 siRNA treated (bottom) cells (left). All images are sum intensity projections of five z-planes. Graph (right) shows PRC1 intensity in untreated (magenta) and PRC1 siRNA treated (green) cells. Numbers inside bars; number of cells. (**F**) Spindle in a fixed unlabeled untreated HeLa cell (top left) and HeLa BAC cell expressing MKLP1-GFP (bottom left), immunostained for MKLP1 (AF-594, green), PRC1 (AF-647, magenta) and stained with DAPI (not shown). Images are sum-intensity projections of 5 z-planes smoothed with 0.5-pixel-Gaussian blur. Graph (right) shows MKLP1 intensity in untreated unlabeled (magenta) and BAC cells (green). The signal intensity of MKLP1 in these cells was 6% higher compared to endogenous MKLP1. (**G**) Time-lapse of HeLa BAC cell expressing MKLP1-GFP, depleted for endogenous PRC1, with transient expression of opto-PRC1 and iLID-CAAX (only MKLP1-GFP is shown) in time-points as in **Fig. 4 A** (top). Graphs (middle) correspond to membrane-to-membrane intensity profiles of MKLP1-GFP (green) and opto-PRC1 (magenta) retrieved from the same position perpendicular to the midzone in time-points as in **Fig. 4 A**, acquired by 1-µm wide line on maximum projection of three z-planes. Schematic representation of performed measurement is given on the right. Graphs (bottom) show individual MKLP1-GFP (left) and opto-PRC1 (right) intensities. Scale bars; 2 µm.

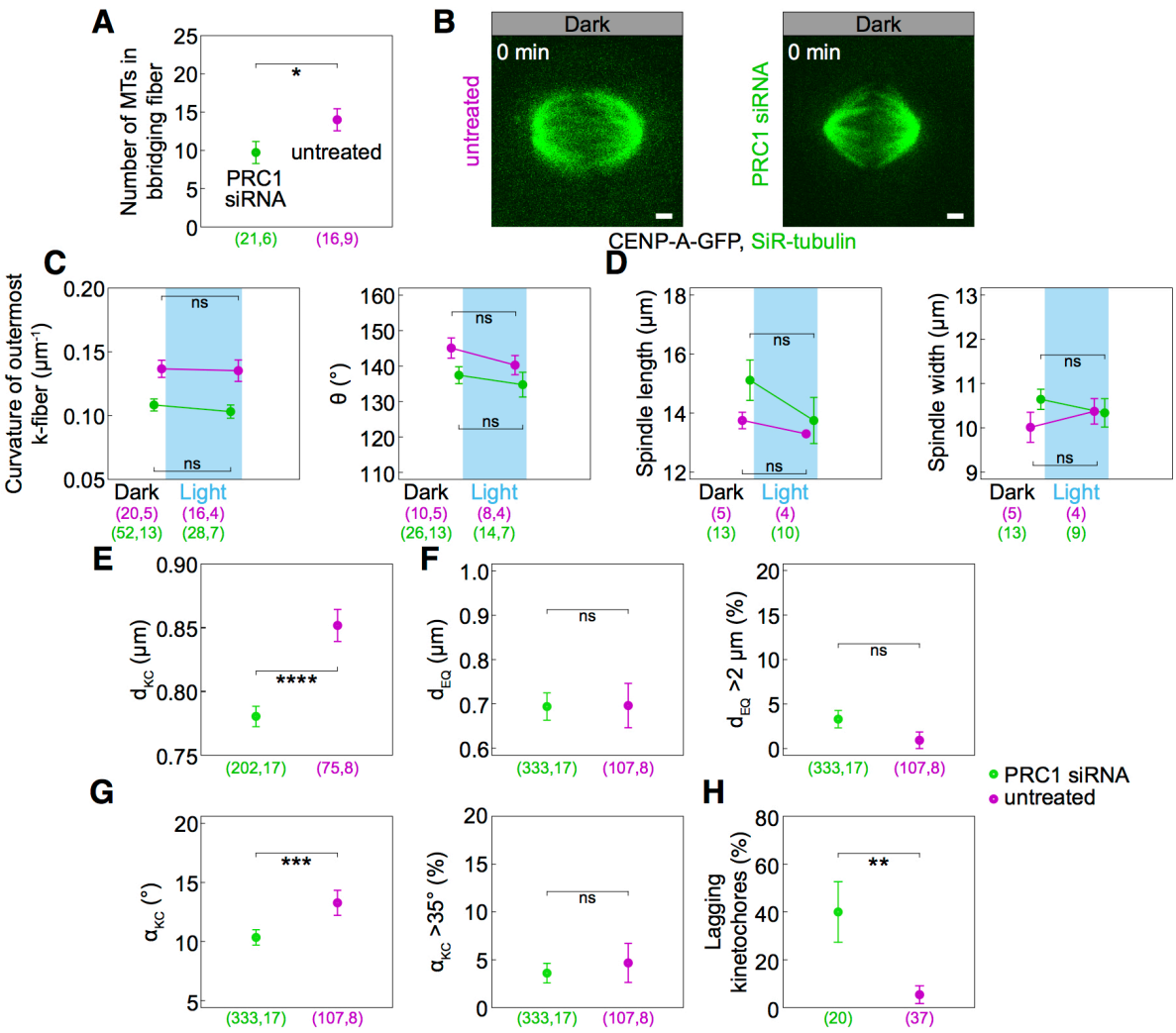


**Figure S5.**

(**A**) Number of microtubules in the bridging fiber in untreated (magenta) and PRC1 siRNA treated HeLa cells (green) retrieved from our previous study(Polak et al., 2017). (**B**) Spindles of untreated (left) and PRC1 siRNA treated (right) U2OS cells with stable expression of CENP-A-GFP (not shown) and stained with SiR-tubulin (green) (**C**) Curvature (left) and angle between (right) the outermost k-fibers in cells as in **B**, untreated (magenta) or PRC1 siRNA treated (green), before (0 min, Dark) and at the end of continuous exposure to the blue light (20 min, Light). (**D**) Spindle length (left) and width (right) in cells as in **B**. (**E**) Measurements of $d_{KC}$ in untreated (magenta) and PRC1 siRNA treated (green) U2OS cells with stable expression of CENP-A-GFP and stained with SiR-tubulin. (**F**) Measurements of $d_{EQ}$ in cells as in **B** (left) and percentage of $d_{EQ}$ greater than 2 μm (right) in untreated (magenta) and PRC1 siRNA treated (green) cells. (**G**) Measurements of $\alpha_{KC}$ in cells as in **B** (left) and percentage of $\alpha_{KC}$ greater than 35° (right) in untreated (magenta) and PRC1 siRNA

treated (green) cells. (**H**) Occurrence of lagging kinetochores in anaphase of untreated (magenta) or PRC1 siRNA treated (green) U2OS cells with stable expression of CENP-A-GFP and stained with SiR-tubulin.
Cyan rectangles inside graphs indicate exposure to the blue light. Numbers and single numbers in brackets are measurements and cells, and cells, respectively. Scale bars: 2 µm. Statistical analysis; t-test (**A**, **C-E**), Man Whitney test (**F** and **G**, left), two-proportions z-test (**F** and **G**, right; **H**); p-value legend as in **Fig. 2**.

**Video Captions**

**Video 1.**
U2OS cell stably expressing CENP-A-GFP (cyan), with transient expression of opto-PRC1 (magenta) and iLID-CAAX. The time of exposure to the blue light is indicated in the upper right corner. Time; min:s. The video corresponds to still images from **Fig. 1 B**.

**Video 2.**
Unlabeled U2OS cell with transient expression of opto-PRC1 (magenta) and iLID-CAAX, and chromosomes stained with SiR-DNA (blue). The time of exposure to the blue light is indicated in the upper right corner. Time; min. The video corresponds to still images from **Fig. 2 A.**

**Video 3.**
U2OS cell stably expressing CENP-A-GFP (cyan), with transient expression of opto-PRC1 (magenta) and iLID-CAAX. Note the kinetochores moving further from the equatorial plane upon PRC1 removal. The time of exposure to the blue light is indicated in the upper right corner. Time; min:s. The video corresponds to still images from **Fig. 2 C**.

**Video 4.**
U2OS cell stably expressing CENP-A-GFP (cyan), with transient expression of opto-PRC1 (magenta) and iLID-CAAX, and microtubules stained with SiR-tubulin (green). Note the kinetochores lagging in the spindle midzone after anaphase onset. The time of exposure to the blue light is indicated in the upper right corner. Time; min. The video corresponds to still images from **Fig. 2 I**.

**Video 5.**

U2OS cell stably expressing CENP-A-GFP (not shown), with transient expression of opto-PRC1 (magenta) and iLID-CAAX, and microtubules stained with SiR-tubulin (green). The time of exposure to the blue light is indicated in the upper right corner. Top: SiR-tubulin; bottom: merge. Time; min. The video corresponds to still images from **Fig. 3 B** and **Fig. S3 A**.